TECHNICAL REPORT 4800

PENETRATION OF A TRANSPARENT MEDIUM BY RIGID BLUNT-AND CONICAL-NOSED BODIES OF REVOLUTION

SIDNEY S. JACOBSON

DECEMBER 1975

PICATINNY ARSENAL

DOVER, NEW JERSEY

The findings in this report are not to be construed as an official Department of the Army Position.

DISPOSITION

Destroy this report when no longer needed. Do not return to the originator.

UNCLASSIFIED

SECURITY CLASSIFICATION OF THIS PAGE *(When Data Entered)*

REPORT DOCUMENTATION PAGE		READ INSTRUCTIONS BEFORE COMPLETING FORM
1. REPORT NUMBER Technical Report 4800	2. GOVT ACCESSION NO.	3. RECIPIENT'S CATALOG NUMBER
4. TITLE *(and Subtitle)* Penetration of a Transparent Medium By Rigid Blunt- And Conical-Nosed Bodies of Revolution		5. TYPE OF REPORT & PERIOD COVERED Final 6. PERFORMING ORG. REPORT NUMBER
7. AUTHOR(s) Sidney S. Jacobson		8. CONTRACT OR GRANT NUMBER(s)
9. PERFORMING ORGANIZATION NAME AND ADDRESS Ammunition Development & Engineering Directorate Picatinny Arsenal, Dover, New Jersey		10. PROGRAM ELEMENT, PROJECT, TASK AREA & WORK UNIT NUMBERS
11. CONTROLLING OFFICE NAME AND ADDRESS		12. REPORT DATE December 1975 13. NUMBER OF PAGES 61
14. MONITORING AGENCY NAME & ADDRESS*(if different from Controlling Office)*		15. SECURITY CLASS. *(of this report)* Unclassified 15a. DECLASSIFICATION/DOWNGRADING SCHEDULE

16. DISTRIBUTION STATEMENT *(of this Report)*

17. DISTRIBUTION STATEMENT *(of the abstract entered in Block 20, if different from Report)*

Approved for public release; distribution unlimited.

18. SUPPLEMENTARY NOTES

19. KEY WORDS *(Continue on reverse side if necessary and identify by block number)*

Kinetic energy penetration	Experimental impact study
Ductile penetration	Terminal ballistics
Penetration mechanics	Polycarbonate target
Penetration trajectory	High speed photography of trajectory

20. ABSTRACT *(Continue on reverse side if necessary and identify by block number)*

An experimental method of studying impact and penetration was devised to find the deceleration of a penetrator impacting a target at striking velocities of 1500 to 2500 feet per second. Throughout the experimentation, transparent polycarbonate plastic was used as the target material and rigid steel projectiles with blunt or conical noses were used as penetrators. Distance-time data for the penetrator tip, recorded on high-speed film, was reduced to polynomial form. The results were

DD FORM 1 JAN 73 1473 EDITION OF 1 NOV 65 IS OBSOLETE

UNCLASSIFIED

SECURITY CLASSIFICATION OF THIS PAGE *(When Data Entered)*

20. Abstract (Continued)

compared with a theory based on the forces on the penetrator generated by the inertia, compression, and friction of the target. There was reasonably good agreement between the theory and the numerically fitted measured data. In addition, certain phenomena were observed in the target which might delineate the elastic-plastic interface caused by penetration.

ACKNOWLEDGMENTS

This work was done while the author attended Princeton University on an Educational Fellowship provided by Picatinny Arsenal. The actual experiments were conducted at Picatinny, using the facilities of the Technical Support Directorate (TSD) and equipment provided by the Feltman Research Laboratory (FRL).

The author is indebted to Professor A. C. Eringen, of Princeton, for assistance in theoretical analysis, guidance in experimental work, and many valuable discussions. Appreciation is also expressed to Dr. R. H. Scanlon for his review of the manuscript.

The experimental effort was greatly aided by the technicians in TSD, particularly Messrs. L. Bercow, J. Kocur, A. Kocur, R. Wack, and J. Stark. Use of the xenon flash unit was made possible through the co-operation of Dr. E. N. Clark and Mr. I. P. Juriaco of FRL. Mr. G. Randers-Pehrson, also of FRL, assisted in programming and computation.

TABLE OF CONTENTS

INTRODUCTION

The impact of two bodies and the phenomenon of the penetration of one by the other has been studied by physicists and engineers for many years. However, the development of a comprehensive theory explaining the phenomenon has been hampered by the variety of parameters found in both the penetrator and the target, and by the difficulty in quantifying and analyzing the mechanical processes involved in the penetration event.

The purpose of this report is not to propose a comprehensive theory, but to record the results of an experimental approach to one area of the problem: the analysis of the forces acting on the penetrator during its travel through the target. It is hoped that the results of the experiment, and the photographic technique employed, will be useful in the continuing development of the theory of penetration.

GENERAL DISCUSSION

Of the various parameters (Table 1) that affect penetration behavior, those connected with variation in velocity produce the most fundamental changes in the types of penetration that occur (Ref 1). In the order of increasing velocity, the types of impact may be classified as elastic, plastic, and hydrodynamic.

Elastic Impact

At low velocities (the limiting velocity is dependent on the shape of the penetrator and the density of both penetrator and target), the impact is fully elastic, and stresses in both the target and penetrator do not exceed the elastic limit. Only a small part of the kinetic energy of the penetrator is converted into elastic waves in the target; the majority is converted to elastic strain. After the projectile stops moving, the target deformation is reversed and the stored strain energy is returned to the projectile as rebound kinetic energy.

Plastic Impact

As the velocity of impact increases, reaching a critical level for a particular set of geometric and material conditions, permanent deformations of the target and/or penetrator occur. The stress level exceeds the yield point, first locally, at the point of impact, and then, as the velocity is further increased, in a larger and larger volume of the material. The

Table 1

Primary penetration input parameters

Penetrator	Material properties	
	Density (specific weight)	
	Hardness	
	Strength	
	Shear yield	σ_s
	Tensile yield	σ_t
	Compressive yield	σ_c
	Moduli	
	Elastic	E_p
	Shear	G_p
	Bulk	K_p
	Poisson's ratio	ν_p
	Isotropy or anisotropy	
	Geometry	
	Shape of initially impacting surface (nose shape)	
	Volume (mass)	
	Impact velocity	V_i
Target	Material properties	
	Density (specific weight)	ρ_T
	Hardness	
	Strength	
	As above	$\sigma_{s,t,c}$
	Moduli	
	As above	E_T, G_T, K_T
	Poisson's ratio	ν_T
	Isotropy	
	Geometry	
	Obliquity (angle with respect to impacting penetrator trajectory. Normal impact = 0)	
	Thickness	
	External dimension	

impact velocity at which initial plastic deformation occurs is determined by the shape of the penetrator. Certain shapes (such as cones with small vertex angles) cause stress concentrations at lower velocities than do blunt cylinders or spheres. At velocities considerably above the critical velocity for plastic yielding, more and more of the kinetic energy of the penetrator is converted into plastic working of the target, and the work expended on the elastic deformations forms a smaller proportion of the total effect on the target.

Hydrodynamic Impact

As the impact velocity increases to a level where the stresses caused by impact become significantly greater than the yield stress, the hydrodynamic regime of penetration comes into play. At this stress level, the material of the projectile or target (or both) appears to act as a fluid and the densities of the materials govern the mechanics of the impact. The penetration of explosively formed metallic jets into metallic media exemplifies this regime. The theories developed by Birkhoff, et al (Ref 2) and Tate (Ref 3 and 4), are based on a Bernoulli equation which balances pressures on both sides of the moving interface between penetrator and target. In the target, the lower limit of the impact velocity for this regime depends on how rapidly the yield strength of the material is reached during penetration. The yield strength concerned is the dynamic one, which can vary from the static loading condition. As a result, when the yield strength of a material increases with increasing rate-of-strain, the onset of the hydrodynamic regime is delayed until higher stress levels are reached.

Penetrators with kinetic energy imparted by the rapid conversion of chemical energy from propellants or stored energy from compressed or elastically distorted materials have long been used to defeat armor. Until the advent of the practical lined explosive charge, the velocity of impact of penetrators always fell within the plastic regime. Lined explosive charges have raised the impact velocity to the hydrodynamic regime and occasionally to sonic velocities. The plastic regime of impact and penetration is still of great interest, however, and is the subject regime for the experiment described in this paper.

Most research in this area has been concentrated on penetration that results in perforation of the target. There are ample reasons for this since, from an engineering point of view, perforation of the target and exit of the penetrator (intact or otherwise) constitutes defeat of the target. From a more basic point of view, however, the exiting penetrator provides one of the few sources of data from which the dynamics of the penetration process can be inferred. Balancing the momentum or the energy of the incoming penetrator with its existing momentum or energy has been the basis of most of the theories of penetration.

Momentum balance was discussed by Zaid and Paul (Ref 5 and 6) for the perforation of thin plates. Detailed assumptions on the deformed configuration of the perforated plates were made, particularly regarding the shape and extent of exit petalling. From these assumptions, the velocity drop of the exiting penetrator was predicted for thin plates. Correlation between theory and experiment was good for thin plates, but decreased as the plate thickness increased.

For target plates of moderate thickness (approximately the diameter of the penetrator) impacted by blunt penetrators, shearing of a plug is found experimentally to be a primary failure mode of the target. Recht and Ipson (Ref 7) developed predictive equations for plugging failure based on energy considerations which accounted for the deceleration of the penetrator and acceleration of the sheared plug. Predictions made were for a combined penetrator and plug velocity on exit. Correlation was good as long as plate thickness was moderate.

In thick targets, it is necessary to consider the piercing type of penetration as well as plugging. In the case of piercing, target material moves radially from the path of the penetrator and a large zone of plastically deformed material exists around the trajectory of the penetrator. The energy necessary to deform the material in the plastic state was investigated by Bethe (Ref 8) and Taylor (Ref 9). More recently, Awerbuch (Ref 10), Goldsmith and Finnegan (Ref 11), and Awerbuch and Bodner (Ref 12 and 13) have reported on both theory and experiments attempting to quantify the forces acting on the penetrator of thick plates during the stages of piercing and plugging. Again, measurement of residual velocity was the chief source of data from which the resistance forces could be verified. The theory developed by Awerbuch and Bodner (Ref 12) accounts for inertial, compressive, and shear-resistance forces allocated to different parts of the penetration trajectory. Predictions were made of residual

velocities, trajectory times and force-time histories. The results of the experiments conducted (Ref 13) were found to be in good agreement with the analysis (Ref 12).

The details of the penetration process within the target are often elusive. The choice of opaque metallic targets has precluded the use of high speed photographic techniques to record the trajectory of the projectile during penetration. Even the impact phenomenon, in the few microseconds during which the penetrator enters the target, is difficult to capture photographically. Pressures are frequently high enough during the initial stages of impact to cause localized vaporization of the target-penetrator interface; the resultant flash obscures the photographic record.

Radiography can be used effectively to see through the impact flash and record early impact phenomena, but even the most powerful radiographic units cannot satisfactorily record the dynamics of the trajectory of a penetrator as it becomes embedded in a thick metallic target. To minimize boundary effects, the target must be at least five times the diameter of the projectile. The X-ray would have to penetrate both the projectile and the surrounding target material, a thickness beyond most equipment's capability. In addition to this problem, the test set up would have to include a series flash-radiographic unit focused on the penetrator's trajectory.

In an experiment using an array of such units, it would be necessary to sequence the radiographic flashes at intervals of 25-50μ sec, and to place the units and film cassettes so there would be no interference between individual cassettes. If the cassettes were in the path of incoming radiation, each individual film would record the flashes of neighboring X-ray units resulting in "over-writing."

EXPERIMENTAL APPROACH

Selection of Target Material

Because of the difficulty of using radiographic techniques with metallic targets, an experiment was devised to photograph the trajectories of rigid penetrators as they moved through transparent targets. The selection of an appropriate target material required an experimental program in itself. The material had to be of good optical quality, and reasonably similar to metals in its reaction to penetration; that is, it had to be tough enough to withstand impact without fracturing. Experiments with

Table 2

Parameters and test results for Type 2 penetrators

Shot No.	Weight (lb)	Impact velocity (in/sec)	Camera framing rate (frames/sec)	Descriptive results
312181	0.089	18804	24300	Penetrated but swerved. Came to rest at x = 4.21 in.
312182	0.089	22600	24300	Penetrated target completely. No swerve.
403141	0.089	30189	25300	Penetrated target completely. No swerve.
403142	0.089	18396	25200	Penetrated and came to rest at x = 4.46 in. No swerve.
403152	0.089	28872	25600	Penetrated completely. No swerve.
403153	0.089	22248	25400	Penetrated completely. No swerve.

glass, epoxies, and acrylics were unsuccessful. Each was too brittle to accept even low velocity penetrators such as cal .50 bullets, 0.5 inch diameter, traveling at 500 to 1000 fps. Cracks propagated through the material faster than the penetrator, destroying the optical properties of the material, and blanking out the film record.

A polycarbonate plastic known commercially as Lexan 101*, which had reasonably good optical properties, did not shatter on impact, and reacted in many respects like metal, was selected as the target material.

Experimental Setup and Procedure

Following the selection of the target material, the experiment was set up as shown schematically in Figure 1 and in a photograph of the site (Fig 2). A Mann gun using conventional ball propellant and a mechanical firing system was situated with its muzzle approximately four feet from the face of the target block. Manufactured from extruded polycarbonate rod, the target block (Fig 3) was held in a clamping fixture (Fig 4) bolted to the test stand. The penetrators (Fig 5) were made from hardened steel rod. Of the four types of penetrators shown in Figure 5, only the blunt- and conical-nosed (Types 1 and 2) were actually used in the experiment; the other types were designed for future testing.

Impact velocity was obtained by two break-circuit screens and a digital counter-chronograph. Photographic records of each shot were obtained with a high-speed, rotating-drum framing camera with the capability of taking 26,000 pictures per second. The camera shutter was opened manually immediately before the shot was fired. The actual penetration was illuminated from the rear of the target by a xenon flash lamp (Fig 4) triggered by the penetrator's breaking an electrical circuit on its approach to the target. A capacitor bank charged to 2.5 kv provided the energy to fire the lamp which provided a fairly sharp illumination peak that lasted for about 2.5 milliseconds with a brilliance equivalent to 28 flashbulbs (Fig 6).

The projectile, while fired from a rifled gun, was not spin stabilized. It was felt that rotation of the penetrator in the target would complicate the analysis of the penetration. However, without rotation, the projectiles used in the experiment would not be aerodynamically stable, and would begin to tumble over a long period of free flight. To offset this problem, the muzzle of the gun was placed as close as practicable to the target.

*A product of the General Electric Co.

little yaw was detected in most of the shots fired. Obturation of the propellant gases in the gun was accomplished by attaching a small plastic cup to the rear of each projectile.

EXPERIMENTAL RESULTS

Typical film records of individual firings are shown in Figures 7 and 8. The rotation of the camera drum is monitored by a digital counter and the angular speed of the drum is linearly related to the framing rate. The time from frame to frame is the reciprocal of the framing rate. A drum speed of 1,538 rev/sec representing 24,500 frames/sec with a time between frames of 40.8 μsec was used for the sequence of shots shown in Figure 8. The films were read by scaling the block dimensions and measuring the frame-to-frame motion of the penetrator tip. From these readings the instantaneous velocity and deceleration were numerically analyzed.

This report covers data reduction on the trajectories of six Type 2 penetrators, identified as 312181, 312182 (initially designated 12-18-1 and 12-18-2, respectively) and 403141, 403142, 403152, and 403153. The details of these experiments are shown in Table 2. Data on the penetration of Type 1 shot has not been tabulated; however, some aspects of the Type 1 firings are included in this report below.

For each shot, the tip motion was measured from the film sequence on a film reading machine with an attached digital counter. Each frame is 16 mm wide and the target length seen in the frame is six inches. The scale in film reader units (fru) varies, depending on camera position, from 500 to 700 fru per inch. Three readings of each frame's penetrator tip position were taken and averaged. These data were used to compute a fifth degree polynomial fit, $x = x(t)$, by least squares techniques, with the coefficient of the linear term constrained to be the known impact velocity. Numerical differentiation was computed for velocity and force.

From this experimental program, certain interesting general results have been found:

1. Superficially, the polycarbonate plastic acts like metal in the ductile way it accepts the impact and penetration of the steel projectile. Front petals characteristic of ductile penetration in metals appear on the initial impact surface and, in the case of a perforation, ductile petalling is seen on the rear surface (Fig 9). As the shot penetrates the target,

only minor cracking precedes the penetrator. The material forward of the tip, particularly in the case of conical-nosed projectiles, does not seem to be disturbed.

2. A zone of highly disturbed material exists in the track of the penetrator. The hole that the penetrator makes becomes smaller than the penetrator immediately after the penetrator has passed. This is evident in Figure 8, frames 7 through 14. The material immediately adjacent to the trajectory hole is highly crazed and appears to be the result of the plastic's melting and recrystalizing (Fig 10). The crazed zone and the hole itself are opaque.

3. An interesting region surrounding the crazed material is shown in Figures 9 and 10. In Figure 9, a transparent volume of material (about 2.5 penetrator diameters) surrounds the hole made by the penetrator. In Figure 10, the transparent region is in two parts. A curved surface extends from the projectile tip to about two penetrator diameters beyond the rear of the penetrator. The diameter of the surface is about three times the diameter of the penetrator. It shrinks, subsequently, to about three times the residual hole diameter, and maintains that diameter almost to the point of entrance. Most interesting is the distinctive boundary between the two transparent portions of the target material. It is speculated that the material inside the boundary has been worked plastically, since the boundary surface is the elastic-plastic interface. An experiment was conducted to determine if the change in refraction that made the surface visible were due to internal stress alone or to stress heating from the plastic work's changing the optical properties of the material. The surface is only slightly visible in frames 7 through 22 (Fig 8), but can be seen advancing from frame to frame with the moving penetrator. The experiment was conducted with a tensile testing machine in which a Type 2 projectile was slowly pushed into a block of polycarbonate. It was observed that a similar surface was generated in the polycarbonate at a movement rate of 0.1 in./min. However, the diameter of the surface increased to the diameter of the block (more than 6 penetrator diameters). Since only negligible heating of the block occurred in the test, it appeared that the surface was caused by stressing alone. It was also observed that as the impact velocity of the shot increased in the firing tests, the interface surface diameter decreased, suggesting that the effect is due to the viscoelastic and viscoplastic properties of the polycarbonate.

ANALYSIS OF THE EXPERIMENTAL APPROACH

The behavior of the penetrator during its passage through the target is governed by a force system that is extremely complex. In an attempt to model the force and velocity history of the trajectory and to correlate the experimental data already obtained in the penetration of polycarbonate targets, an analysis was made of the specific conditions existing during the experimental firing of Type 2 penetrators.

In the initial model, both plastic and elastic wave particle motions were neglected. The only forces considered to be acting on the penetrator were those derived from the inertial forces of the target material displaced by the penetrator and by the compression of the target material as the penetrator moved through it. Because of the large ratio of the density of the penetrator material to the density of the target material, 6.6, the mass the target compressed by the penetrator and moving with it has been neglected as mass added to the penetrator. Awerbuch and Bodner (Ref 12) include this added mass of target material as part of the penetrator. However, the targets they considered were steel, with the same density as the penetrator.

The initial analysis considers the forces acting on the conical-tipped Type 2 penetrator, since the best sets of experimental data obtained thus far are for this penetrator. The penetration trajectory has been divided into five regimes with penetration, x, defined as the tip location measured from the face of the target:

1. In regime 1, the penetrator tip enters the target and proceeds to $x = a$, the length of the conical nose.

2. In regime 2, the cylindrical part of the penetrator enters the target and proceeds to $x = b$, the total length of the penetrator.

3. In regime 3, the full penetrator is immersed in the target and proceeds to $x = \ell$, the total length of the target.

4. In regime 4, the penetrator tip emerges from the rear face of the target and proceeds to $x = \ell + a$, the full tip of the penetrator emerged.

5. In regime 5, the cylindrical part of the penetrator emerges from the target and proceeds until the full penetrator emerges at $x = \ell + b$.

The forces on the penetrator imposed by movement through the target are assumed to be only inertial, compressive, and frictional. The force fields are shown in Sketch 1.

Regime 1 $0 < x \leq a$

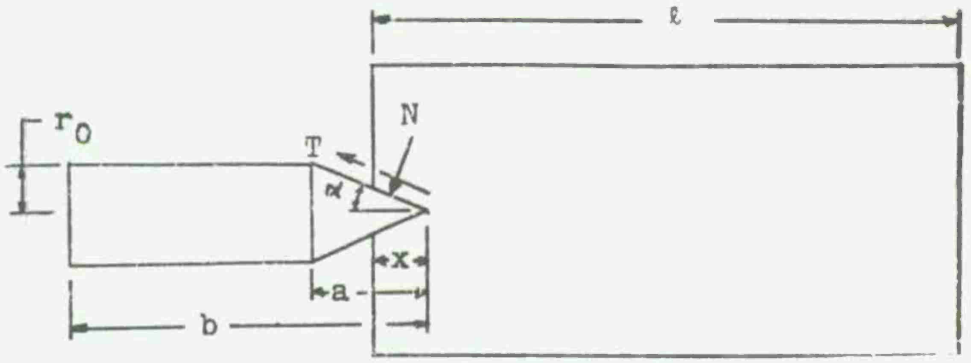

Sketch 1

$$m\frac{d^2x}{dt^2} = -T\cos\alpha - N\sin\alpha \qquad (1)$$

where

$$T = n\,N \qquad (2a)$$

and

$$N = \frac{1}{2}\,\frac{\rho_T}{g}\,A_n\,V_n^2 \qquad (2b)$$

$$= \left[\frac{\pi\rho_T}{2g}\,\frac{\tan\alpha}{\cos\alpha}\,\sin^2\alpha\right]x^2\,\left(\frac{dx}{dt}\right)^2 .$$

Substituting Equation 2 into Equation 1 gives

$$m\,\frac{d^2x}{dt^2} = -A_1\left(\frac{dx}{dt}\right)^2 - B_1 = F_1(x) \qquad (3)$$

where

$$A_1 = \frac{\pi\rho_T}{2g}\,\tan\alpha\,\sin^2\alpha\,(\tan\alpha + n) \qquad (4a)$$

$$B_1 = \pi\sigma_c\,\tan\alpha\,(\tan\alpha + n)\ . \qquad (4b)$$

Integration of Equation 3 with the initial conditions

$$x(0) = 0$$

$$\dot{x}(0) = V_i = \text{initial impact velocity}$$

gives

$$V_1(x) = \left[\left(V_i^2 + \frac{B_1}{A_1} \right) \exp\left(-K_1 x^3\right) - \frac{B_1}{A_1} \right]^{\frac{1}{2}} \tag{5}$$

where

$$K_1 = \frac{2A_1}{3m} .$$

Summing the forces in the x direction gives

$$F_1(x) = -\left(A_1 V_1^2 + B_1\right) x^2 \tag{6}$$

In this development and in the regimes that follow:

1. n is the dynamic friction coefficient between the polycarbonate target and the steel penetrator. An estimate of n from internal reports gathered at Picatinny Arsenal is 0.3 to 0.4, but these data are open to question. Computation of trajectories, however, with the friction coefficient parametrized shows that reasonable fits to the reduced photographic data occur when the friction coefficient is taken as 0.25. This agrees with the known reduction of friction coefficient with the dynamic behavior of materials and may also reflect fluidization of the polycarbonate due to localized melting.

2. ρ_T is the target material density.

3. A_n is the lateral area of the nose of the penetrator subjected to the forces N and T.

4. V_n is the normal velocity of the target material along the surface A_n.

5. a, b, r_o, α, ℓ are penetrator and target geometry parameters defined in Sketch 1.

6. σ_c is the compressive yield strength of the polycarbonate target material. The tensile yield strength of polycarbonate at low rates of loading is given in the literature as 8,000 to 9,000 psi and the compressive yield strength as 11,000 to 12,000 psi (Ref 14). The effects of rate of strain on these values are not well known but are considered to be small (Ref 15). Computation in this report was undertaken with values of σ_c = 11,000 psi.

Regime 2 $a < x \leq b$

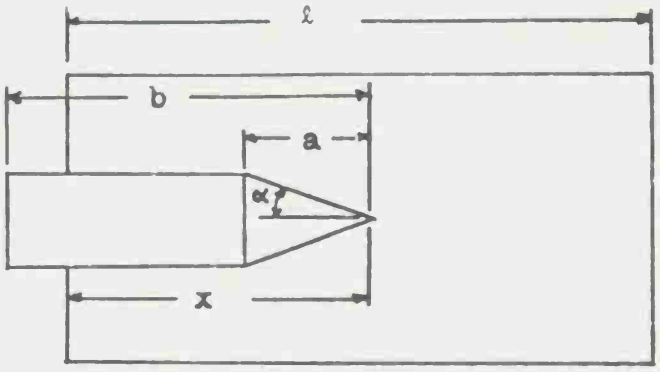

Sketch 2

At the beginning of Regime 2, the retardation force is only on the nose.

$$F_2(a) = A_2 V_a^2 + C_2 \tag{7}$$

where

$$A_2 = \frac{\pi \rho_T}{2g} \sin^2\alpha \tan^2\alpha (\tan\alpha + n) a^2$$

$$C_2 = \pi \sigma_c \tan\alpha (\tan\alpha + n) a^2$$

and

$$V_a^2 = (V_i^2 + \frac{B_1}{A_1}) \exp(-K_1 a^3) - \frac{B_1}{A_1} \tag{8}$$

As x increases from a to b, an additional retardation force caused by friction along the cylindrical body is added to the nose retardation. This force is proportional to the penetration and is a result of the compression acting radially on the cylindrical body.

$$F_2^{\text{body}}(x) = B_2 (x-a) \tag{9}$$

where

$$B_2 = 2\pi n \sigma_c r_o$$

Integration of the differential equation for Regime 2

$$m \frac{d^2x}{dt^2} = -A_2 \left(\frac{dx}{dt}\right)^2 - B_2 (x - a) - C_2 = F_2 (x) \tag{10}$$

with the initial conditions

$$x(a) = a$$

$$\dot{x}(a) = V_a = \text{velocity at a}$$

gives

$$V_2 (x) = \left\{ \left(V_a^2 - \frac{P_2}{K_2} + \frac{C_2}{A_2}\right) \exp[-K_2 (x-a)] - P_2 (x-a) + \frac{P_2}{K_2} - \frac{C_2}{A_2} \right\}^{\frac{1}{2}} \tag{11}$$

where

$$P_2 = \frac{2B_2}{mK_2}$$

$$K_2 = \frac{2A_2}{m} \quad ,$$

and

$$F_2 (x) = A_2 V_2^2 (x) + B_2 (x - a) + C_2 \tag{12}$$

Regime 3 $b < x \leqslant \ell$

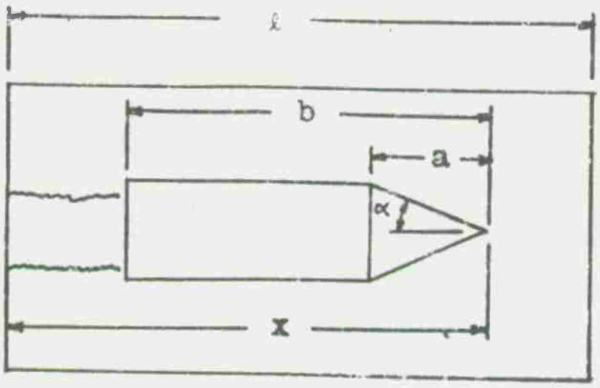

Sketch 3

When the penetrator has fully entered the target, Regime 3 begins. The velocity at the beginning of the regime is V_b, while V_ℓ is the velocity at the end of the regime when the tip location is $x = \ell$. Early in the experimental program, it appeared from photographic evidence of Shot 312182 that the velocity of the penetrator increased slightly on emergence. It was initially conjectured that elastic energy in the target caused a force on the rear of the penetrator. As a first approximation, it was assumed that this force was $\sigma_c A_r$ where σ_c was the appropriate compressive yield strength of the target material and A_r was an area on the penetrator base acted on by this pressure. Calculations which include this force show an increase in the velocity of the penetrator upon emergence from the target; however, physical inconsistencies arise when the behavior of the target-penetrator interface is examined closely (see Sketch 4).

Since the projectile base is square, the motion of the compressed target material flowing around the square corner of the base would have to be physically discontinuous in order to provide material that could press on the base surface of the penetrator.

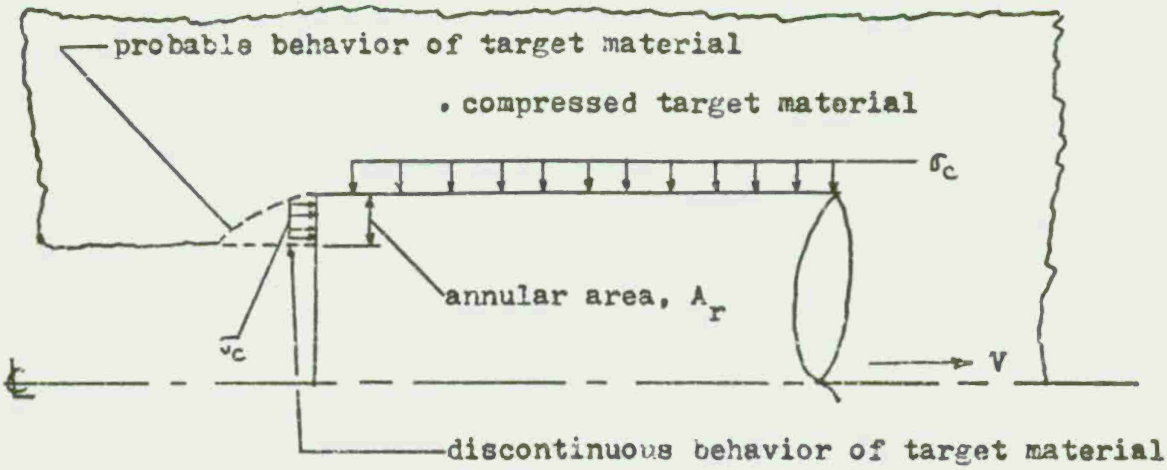

Sketch 4

Other sources of a force that could produce an increase in velocity upon emergence were not examined. Since subsequent shots did not show evidence of such a velocity increase, the computations appearing in this report (Fig 11 through 16) omit the action of such a force on the rear of the penetrator.

The force summary in Regime 3 is

$$F_3(x) = A_2 V_3^2(x) + P_3 = -mV_3 \frac{dV_3(x)}{dx} \qquad (13)$$

where

$$P_3 = B_2(b - a) + C_2$$

Integration of Equation 13 leads to

$$V_3(x) = \left[\left(V_b^2 - \frac{Q_3}{K_2} \right) \exp\left[-K_2 (x-b) \right] + \frac{Q_3}{K_2} \right]^{\frac{1}{2}} \qquad (14)$$

where

$$Q_3 = -\frac{2}{m} P_3$$

and

$$V_b = \left\{ \left(V_a^2 - \frac{P_2}{K_2} + \frac{C_2}{A_2} \right) \exp\left[-K_2 (b-a) \right] - P_2 (b-a) + \frac{P_2}{K_2} - \frac{C_2}{A_2} \right\}^{\frac{1}{2}}$$

$V_3(x)$ is used for the determination of $F_3(x)$. At $x = b$, $V_3(b) = V_b$ and at $x = \ell$, $V_3(\ell) = V_\ell$.

$$V_\ell = [(V_b^2 - \frac{Q_3}{K_2})\exp[-K_2(\ell-b)] + \frac{Q_3}{K_2}]^{\frac{1}{2}} \qquad (15)$$

Regime 4 $\ell < x \leq \ell + a$

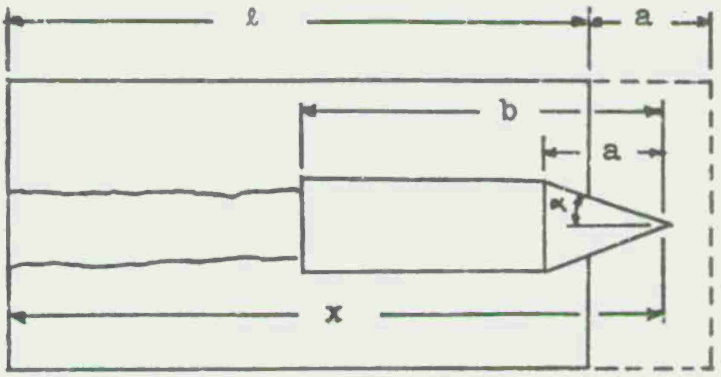

Sketch 5

In the fourth regime, the projectile tip emerges from the target and no resistance force acts on it. In computing the forces it was considered first that the projectile was immersed fully in a target of length x, where $\ell < x \leq \ell + a$. The resultant force, $F_4'(x)$, would be of the same form as in the force in Regime 3,

$$F_4'(x) = A_2 V_3^2(x) + P_3 \qquad (16)$$

From this, a force, $F_4''(x)$, is subtracted which is the force acting on the tip that enters the regime $\ell < x \leq \ell + a$. The emerged tip may be thought of as entering a region similar to Regime 1 with an initial velocity, however, of V_ℓ which is the velocity attained by the penetrator at the end of Regime 3.

$$F_4''(x) = (A_1 \bar{V}_1^2(x) + B_1)(x-\ell)^2 \qquad (17)$$

where

$$\bar{V}_1^2 = (V_\ell^2 + \frac{B_1}{A_1})\exp[-K_1(x-\ell)^3] - \frac{B_1}{A_1}. \qquad (18)$$

$F_4(x)$ would then be

$$F_4(x) = F_4'(x) - F_4''(x) \tag{19}$$

or

$$-mV_4(x)\frac{dV_4(x)}{dx} = A_2\left[\left(V_b^2 - \frac{Q_3}{K_2}\right)\exp[-K_2(x-b)] + \right. \tag{20}$$

$$\left. + P_3 - \left\{A_1\left[\left(V_\ell^2 + \frac{B_1}{A_1} + \frac{B_1}{A_1}\right)\exp[-K_1(x-\ell)^3] - \frac{B_1}{A_1}\right] + B_1\right\}(x-\ell)^2\right],$$

From the solution of the differential equation for Regime 4,

$$V_4(x) = \left\{V_\ell^2 + \frac{2A_4}{mK_2}\left[\exp(-K_2(x-b)) + D_4\right] + \frac{2B_4}{3mK_1}\left[\exp(-K_1(x-\ell)^3) - 1\right] + \right.$$

$$\left. - \frac{2C_4}{m}(x-\ell)\right\}^{\frac{1}{2}} \tag{21}$$

Grouping Equation 20 gives

$$F_4(x) = A_4\exp[-K_2(x-b)] + B_4(x-\ell)^2\exp[-K_1(x-\ell)^3] + C_4 \tag{22}$$

where, for Equations 21 and 22

$$A_4 = A_2V_b^2 - \frac{A_2Q_3}{K_2}$$

$$B_4 = -(A_1V_\ell^2 + B_1)$$

$$C_4 = \frac{A_2Q_3}{K_2} + B_2(b-a) + C_2$$

$$D_4 = -\exp[-K_2(\ell-b)].$$

Regime 5 $\ell + a < x \leq \ell + b$

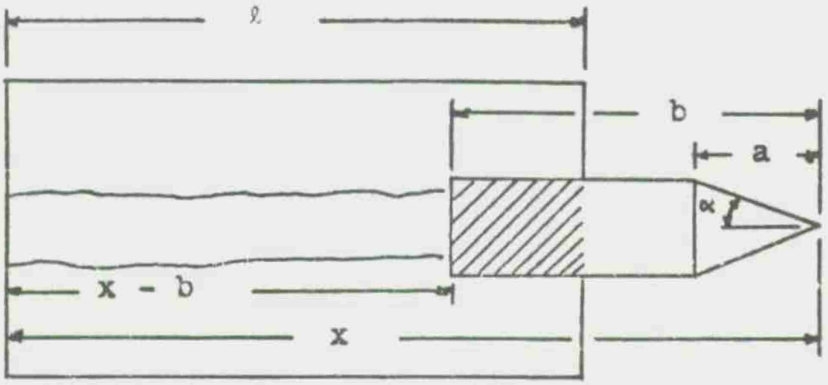

Sketch 6

In this regime, the projectile tip has emerged fully. The forces act only on the cylindrical shaded area of the projectile (Sketch 6). The length of this cylinder on which the forces act is $\ell - (x-b)$

$$F_5(x) = 2\pi n r_0 \sigma_c (\ell + b - x)$$

or

$$-m\, V_5(x)\, \frac{dV_5(x)}{dx} = A_5 x + B_5 \qquad (23)$$

where

$$A_5 = -2\pi\, n r_0 \sigma_c$$

$$B_5 = 2\pi\, n r_0 \sigma_c (\ell + b).$$

Solution of Equation 23 gives

$$V_5(x) = \{V^2_{\ell+a} - \frac{A_5}{m}x^2 - \frac{2B_5}{m}\, x + \frac{A_5(\ell+a)^2}{m} + \frac{2B_5(\ell+a)}{m}\}^{\frac{1}{2}} \qquad (24)$$

where $V_{\ell+a}$ is the velocity at $x = \ell+a$, at the end of Regime 4.

$$V_{\ell+a} = \{V_{\ell}^2 + \frac{2A_4}{mK_2} [\exp(-K_2(\ell+a-b)) + D_4] + \frac{2B_4}{3mK_1} [\exp(-K_1 a^3) - 1] + \frac{2C_4}{m} a\}^{\frac{1}{2}} . \quad (25)$$

At the end of Regime 5, the velocity is

$$V_{\ell+b} = [V_{\ell+a}^2 - \frac{A_5}{m}(\ell+b)^2 - \frac{2B_5}{m}(\ell+b) + \frac{A_5}{m}(\ell+a)^2 + \frac{2B_5}{m}(\ell+a)]^{\frac{1}{2}} \quad (26)$$

This analysis covers the entire trajectory of a conical-tipped penetrator through a polycarbonate target. A series of computations for these five regimes was made to determine the adequacy of the mathematical model when compared with the observed data for a conical-tipped Type 2 penetrator.

Trajectory computations were made on the Picatinny Arsenal CDC 6500 computer in which the relatively unknown quantities σ_c and n were parametrized. The fifth-order polynomials fitted to the photographically observed x, t data were compared to the computed data. Fitting polynomials to points of x, t data leads to difficulty in differentiation where oscillations in the initially fitted curves lead to larger oscillations in the first and second derivatives. Examples of this are shown in Figures 11 through 16 (the curves marked "1" are the differentiated data curves; the "2" curves are derived from the theory).

To overcome the difficulties in curve fitting, an unsuccessful attempt was made to measure the velocity of the penetrating projectile in its trajectory through the plastic target. A small doppler radar was used for several shots to develop a direct velocity readout. The use of the radar was discontinued, however, when it was found that the readings during penetration were overwhelmed by noise due, probably, to stress wave fronts in the plastic that caused the reflections. Because an independent velocity check for a point other than the impact point has not yet been devised, the velocity and force computations must be looked upon as only generally quantitative.

The theoretical force-time curves using σ_c = 11,000 psi and n = 0.25 generally follow the shape of the differentiated data curves except at the end points where the curve fitting is poorest. The sharp changes of slope

in the theoretical force curves indicate the times at which the various regions of penetration begin.

CONCLUSIONS

The experimental techniques described above hold promise as a method of determining the forces of resistance produced in a target by a penetrator. Polycarbonate, while considerably weaker than most metals, exhibits metal-like ductility under impact and penetration, permitting observation and analysis of the trajectory.

The analysis of the trajectory gives a reasonable prediction to the observed data, at least as far as x,t and v,t are concerned. Since the force is obtained from the second derivative, these curves are less reliable. However, the predicted curves do match the general shape of most derived data curves.

REFERENCES

1. Hopkins, H.G. and Kolsky, H., *Mechanics of Hypervelocity Impact of Solids,* Hypervelocity Impact, Fourth Symposium, April 20-28 1960, APGC-TR-60-39, September 1960, Air Proving Ground Center, Eglin Air Force Base, Florida

2. Birkhoff, G., MacDougall, D.P., Pugh, E.M., and Taylor, G.T., *Explosives with Lined Cavities,* Journal of Applied Physics, Vol 19, 1948, P563

3. Tate, A., *A Theory for the Deceleration of Long Rods After Impact,* Journal of the Mechanics and Physics of Solids, Vol 15, 1967, pp 387-99

4. Tate, A., *Further Results in the Theory of Long Rod Penetration,* Journal of the Mechanics and Physics of Solids, Vol 17, 1969, pp 141-50

5. Zaid, M. and Paul, B., *Mechanics of High Speed Projectile Perforation,* Journal of Franklin Institute, Vol 264, 1957, pp 117-126

6. Zaid, M. and Paul, B., *Normal Perforation of Thin Plate by Truncated Projectiles,* Journal of Franklin Institute, Vol 265, 1958 pp 317-335

7. Recht, R.F. and Ipson, T.W., *Ballistic Perforation Dynamics,* Journal of Applied Mechanics, September 1963, pp 384-390

8. Bethe, H.A., *Attempt of a Theory of Armor Penetration,* Frankford Arsenal Internal Report, 1941

9. Taylor, G.I., *The Formation and Enlargement of a Circular Hole in a Thin Plastic Sheet,* Quarterly Journal of Mechanics and Applied Mathematics, Vol 1, 1948, pp 103-174

10. Awerbuch, J., *A Mechanics Approach to Projectile Penetration,* Israel Journal of Technology, Vol 8, 1970, pp 375-383

11. Goldsmith, W. and Finnegan, S.A., *Penetration and Perforation Processes in Metal Targets at and Above Ballistic Velocities,* International Journal of Mechanical Science, Vol 13, 1971, pp 843-866

12. Awerbuch, J. and Bodner, S.R., *Analysis of the Mechanics of Perforation of Projectiles in Metallic Plates,* Israel Institute of Technology, MED Report No. 40, May 1973

13. Awerbuch, J. and Bodner, S.R., *Experimental Investigation of Normal Perforation of Projectiles in Metallic Plates,* Israel Institute of Technology, MED Report No. 42, June 1973

14. Christopher, W.F. and Fox, D.W., *Polycarbonates,* Rheinhold, 1962, p 48

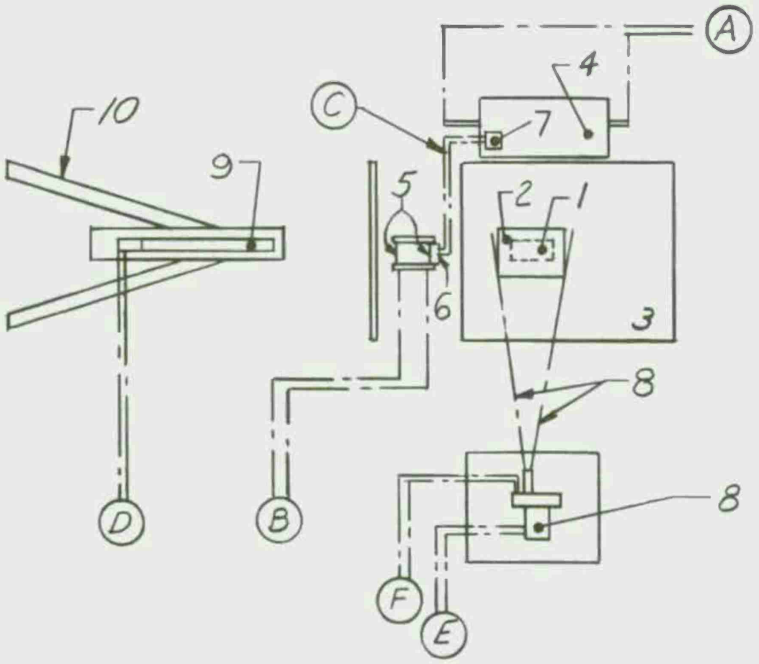

PLAN VIEW SCHEMATIC OF EXPERIMENTAL SETUP

KEY:-

1-TARGET BLOCK
2-TARGET HOLDING FIXTURE
3-TARGET TABLE
4-XENON FLASHLAMP AND PARABOLIC REFLECTOR ASSEMBLY
5-VELOCITY BREAK-CIRCUIT SCREENS AND FRAME
6-FLASHLAMP BREAK-CIRCUIT SCREEN
7-FLASHLAMP TRIGGER
8-HIGHSPEED "DYNAFAX" CAMERA AND FIELD OF VIEW
9-CALIBER 0.50" MANN TYPE GUN
10-GUN MOUNT AND TRAILS

A-TO CAPACITOR BANK POWER SUPPLY
B-TO COUNTER-CHRON-OGRAPH
C-FLASHLAMP TRIGGER CIRCUIT
D-GUN FIRING CIRCUIT
E-CAMERA MOTOR POWER
F-CAMERA SHUTTER TRIGGER

Fig 1 Plan view schematic of experimental setup

Fig 2 Test site and setup

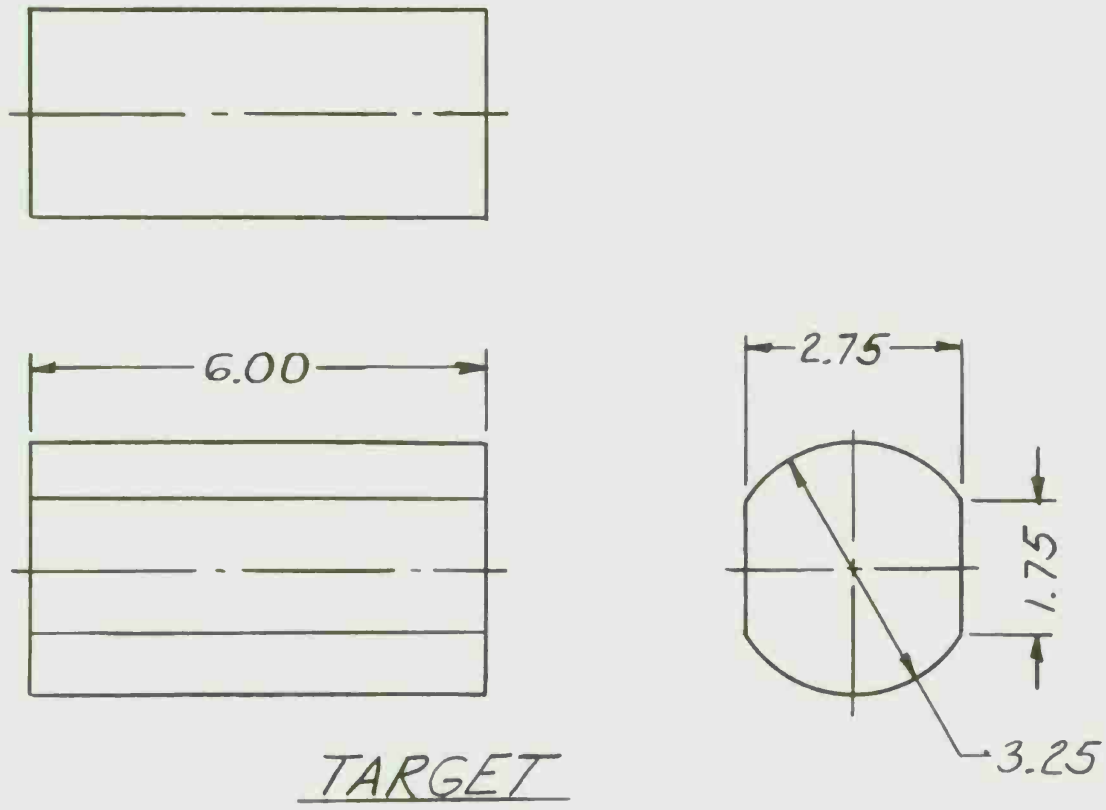

Fig 3 Extruded, polycarbonate rod

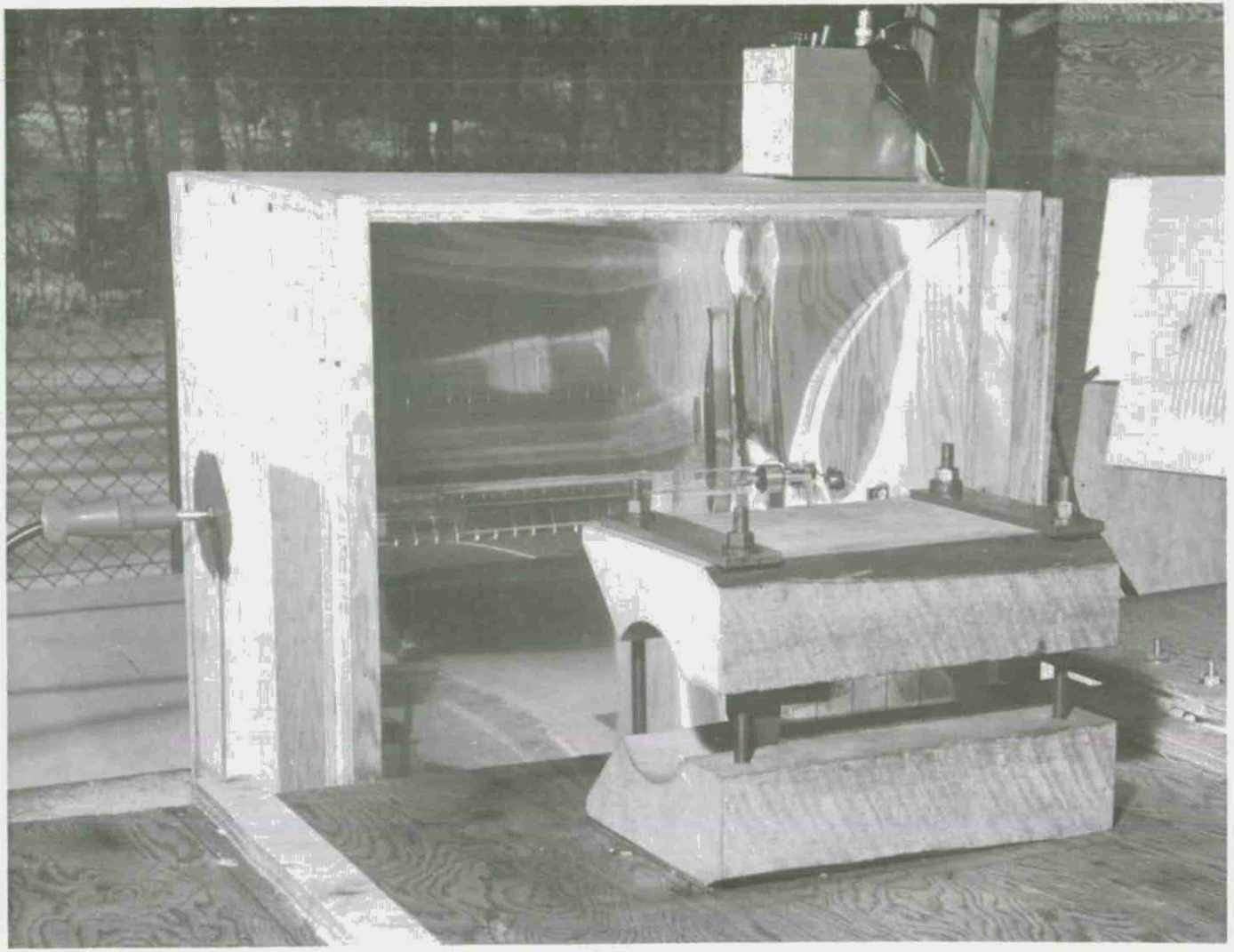

Fig 4 Clamping fixture and Xenon flash lamp showing parabolic reflector

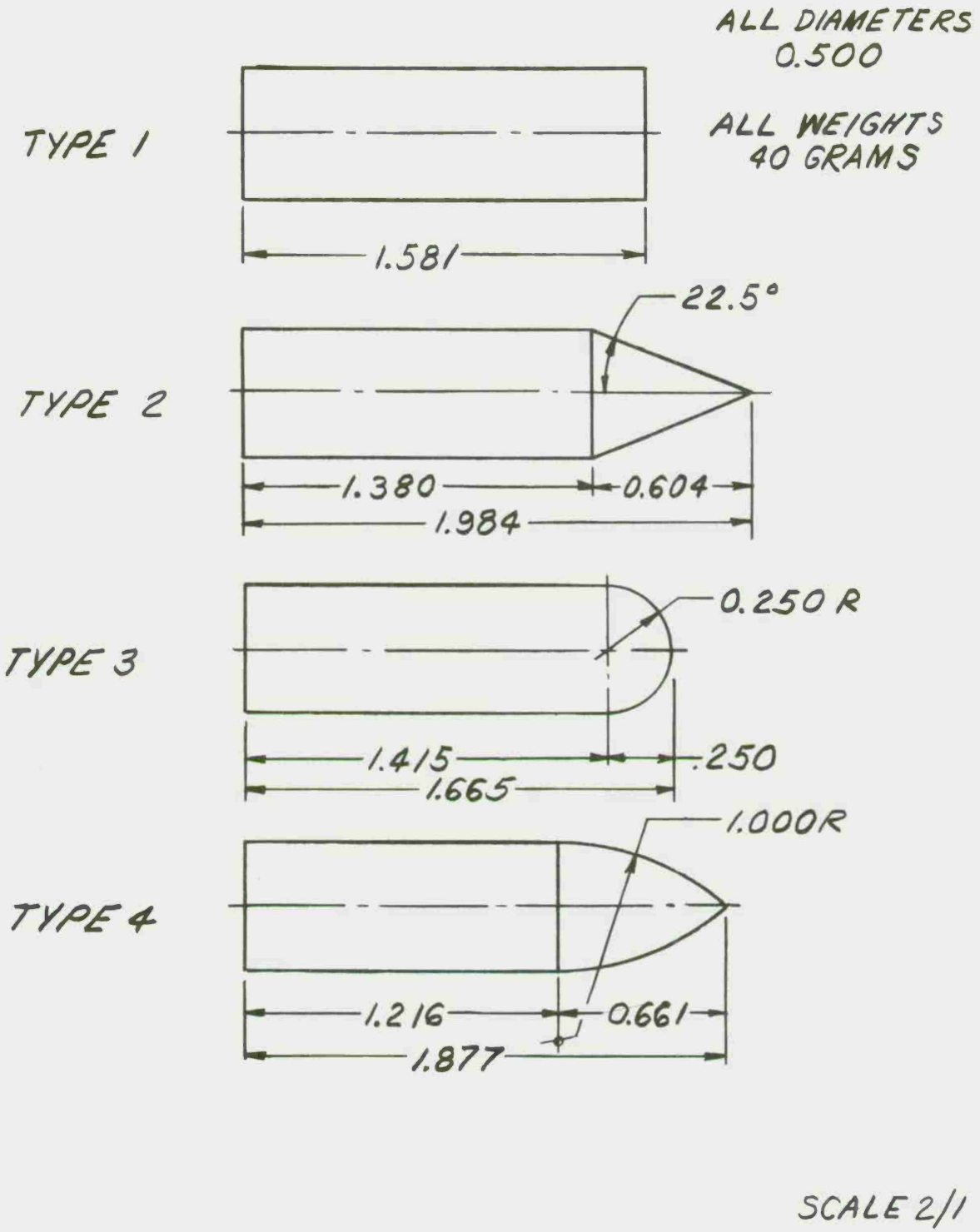

Fig 5 Penetrator designs, Types 1-4

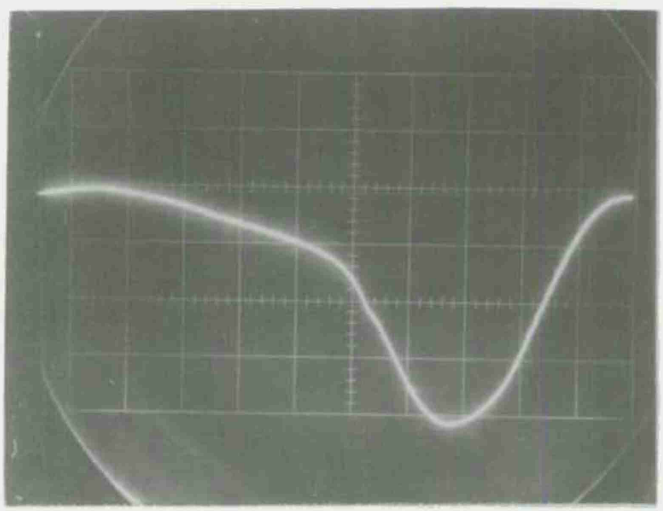

Fig 6 Oscilloscope record of Xenon flash-lamp output. Each abscissa square is 500 μsec and each ordinate square is equivalent to the light intensity of seven flashbulbs

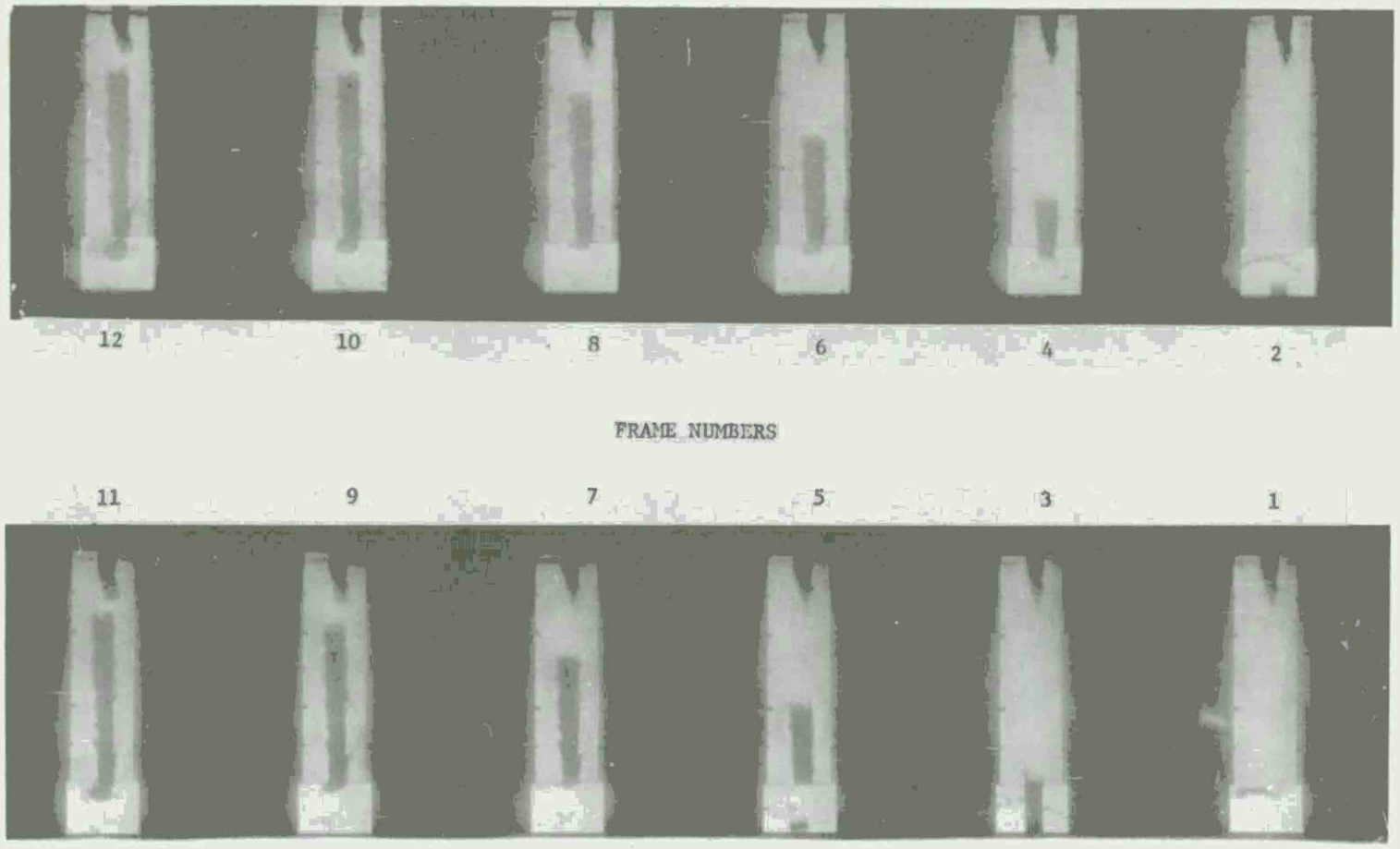

Fig 7 Shot 312111. Sequence of high speed frames of blunt-nosed, Type 1 penetrator trajectory through polycarbonate. Previous penetration seen at top of each frame

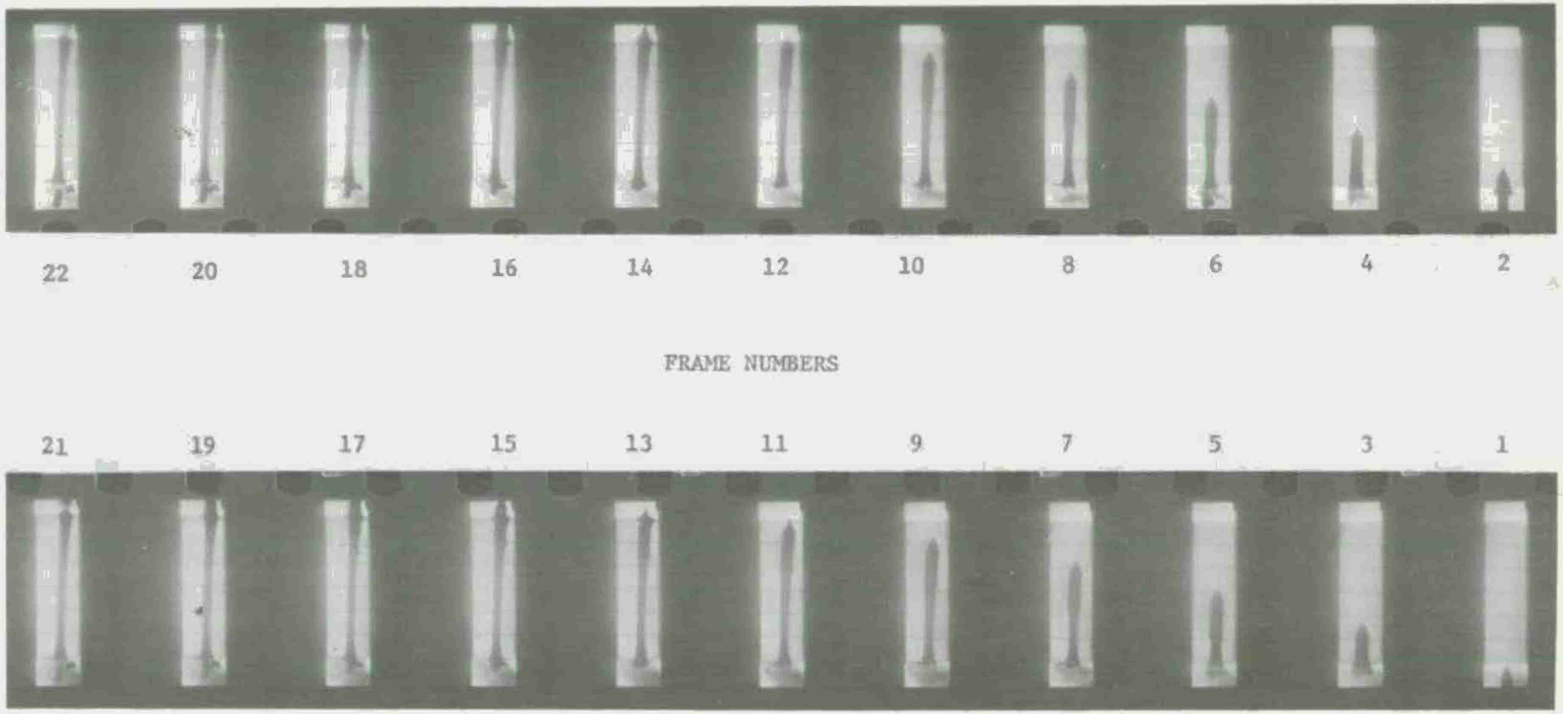

Fig 8 Shot 312182. Sequence of high speed frames of conical-nosed, Type 2 penetrator trajectory through polycarbonate

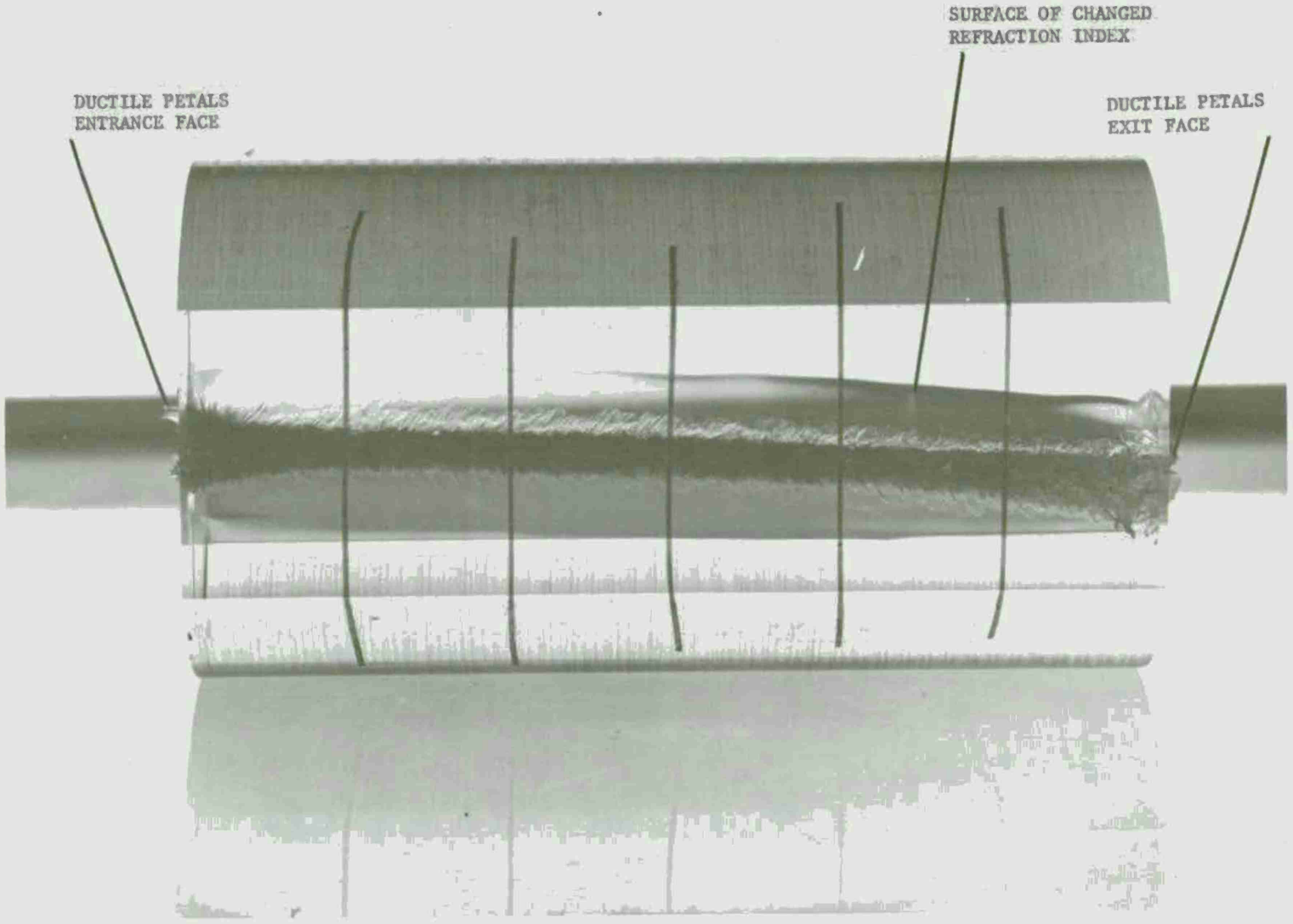

Fig 9 Shot 312182, Type 2 penetrator

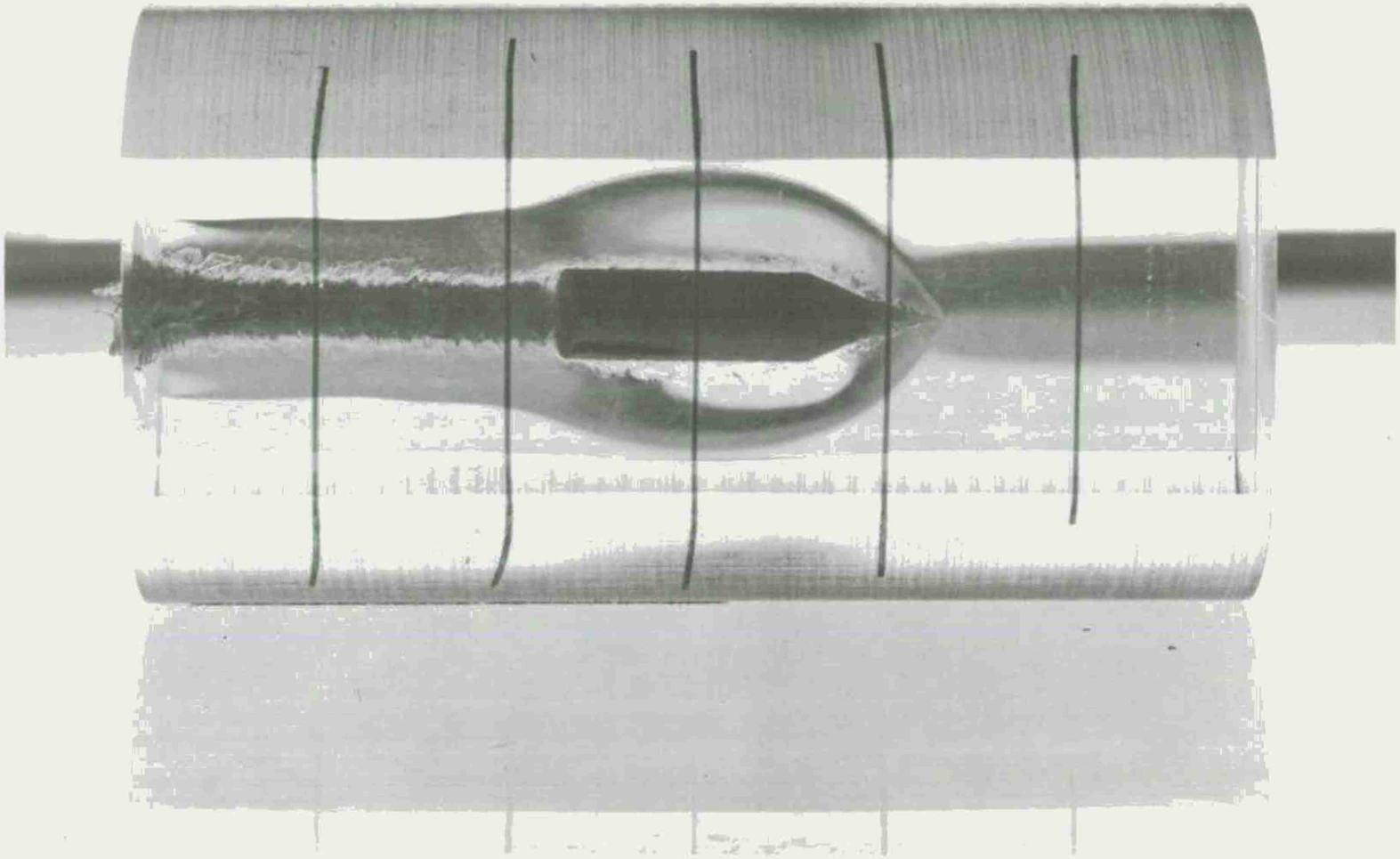

Fig 10 Shot 312181, Type 2 penetrator

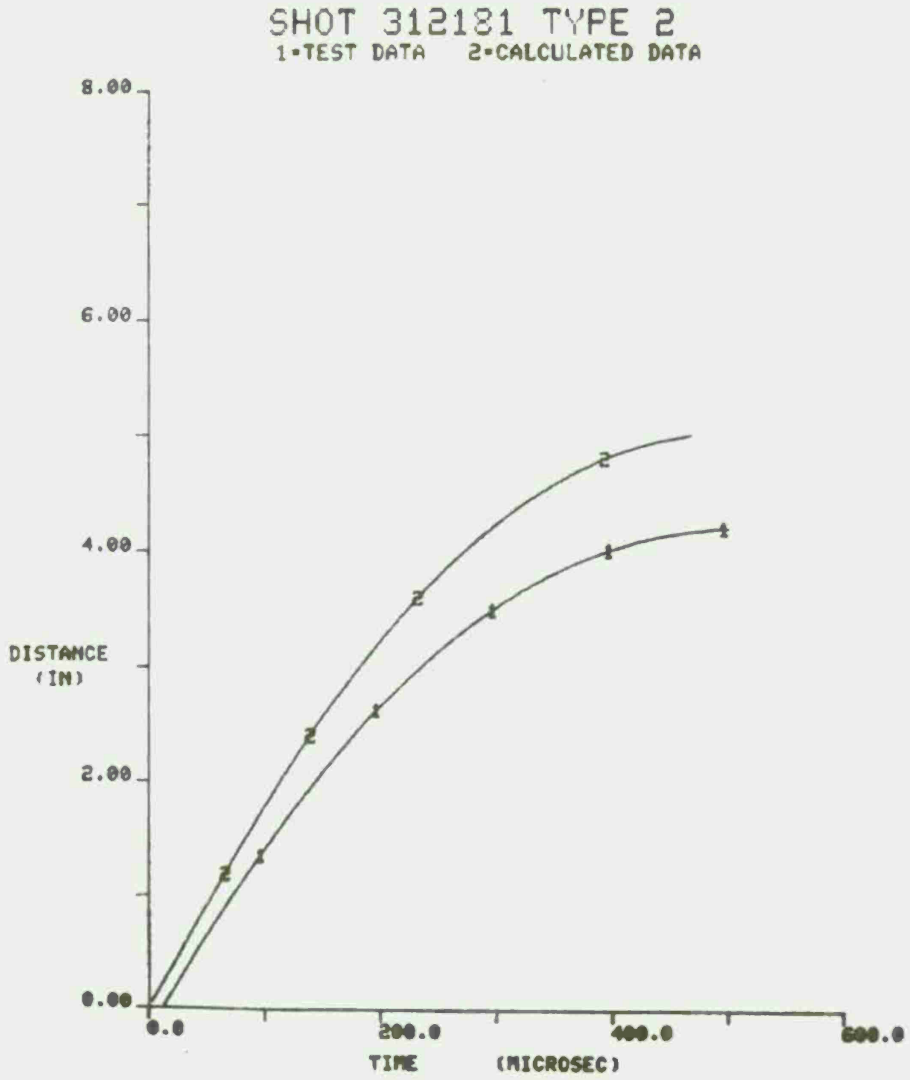

Fig 11a Distance of Type 2, Shot 312181

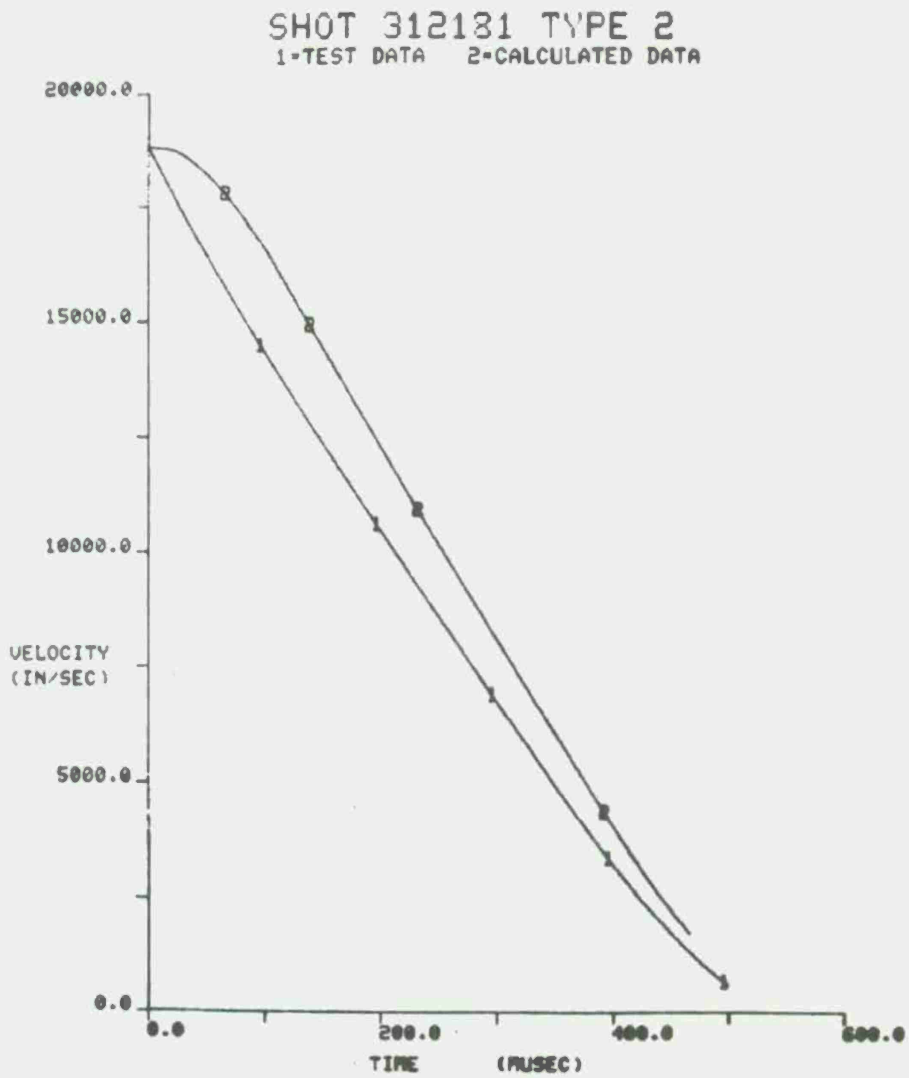

Fig 11b Velocity of Type 2, Shot 312181

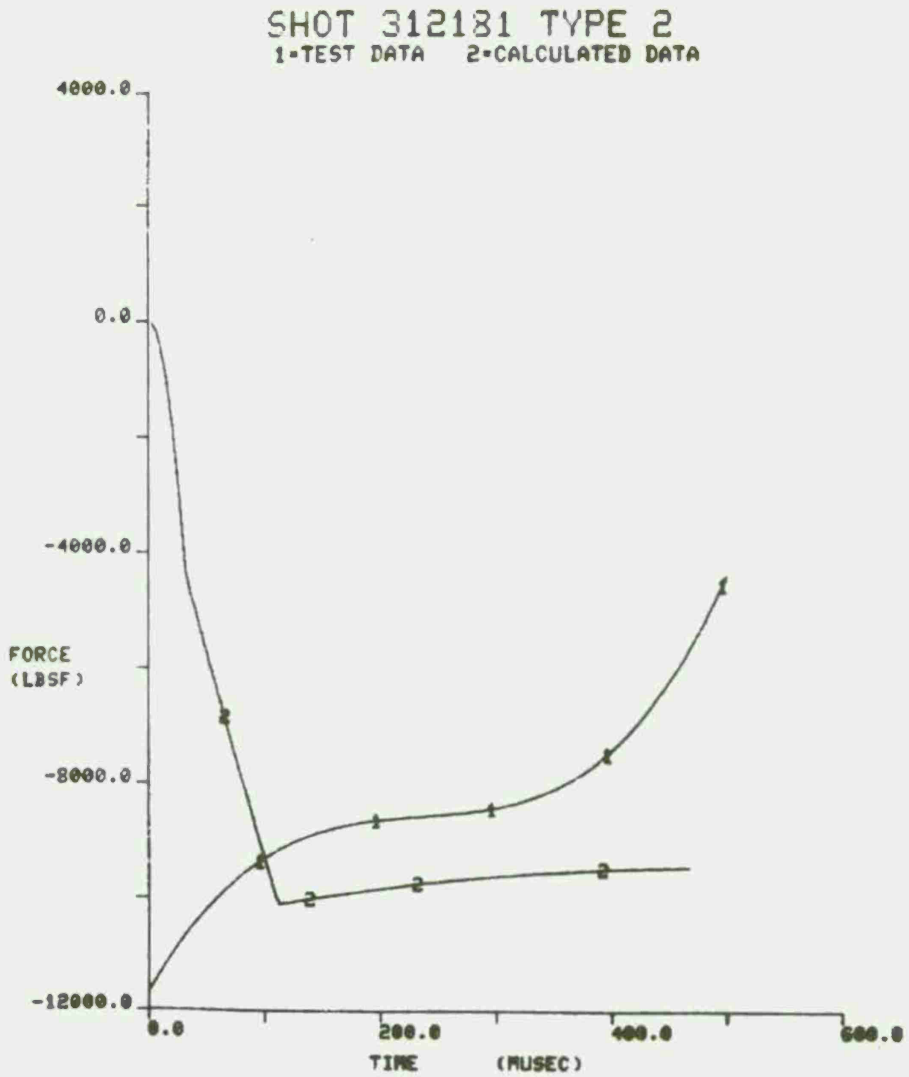

Fig 11c Force of Type 2, Shot 312181

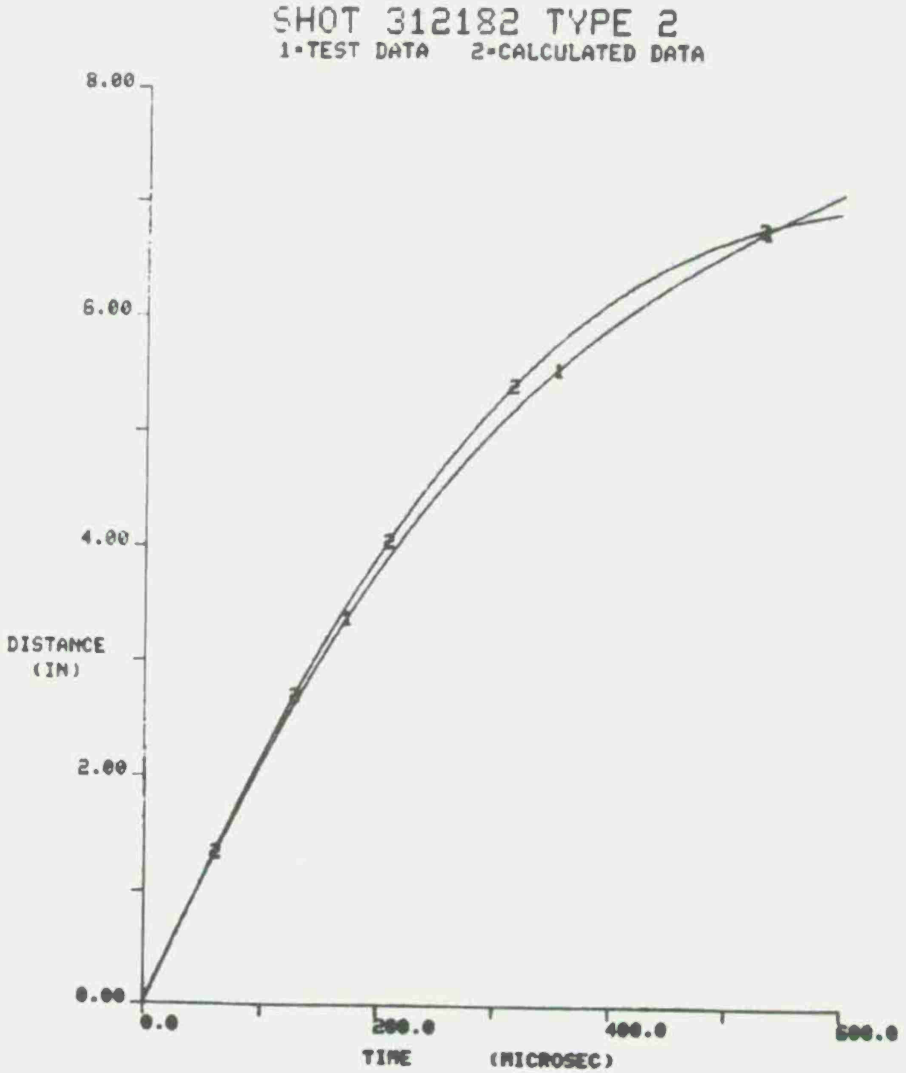

Fig 12a Distance of Type 2, Shot 312182

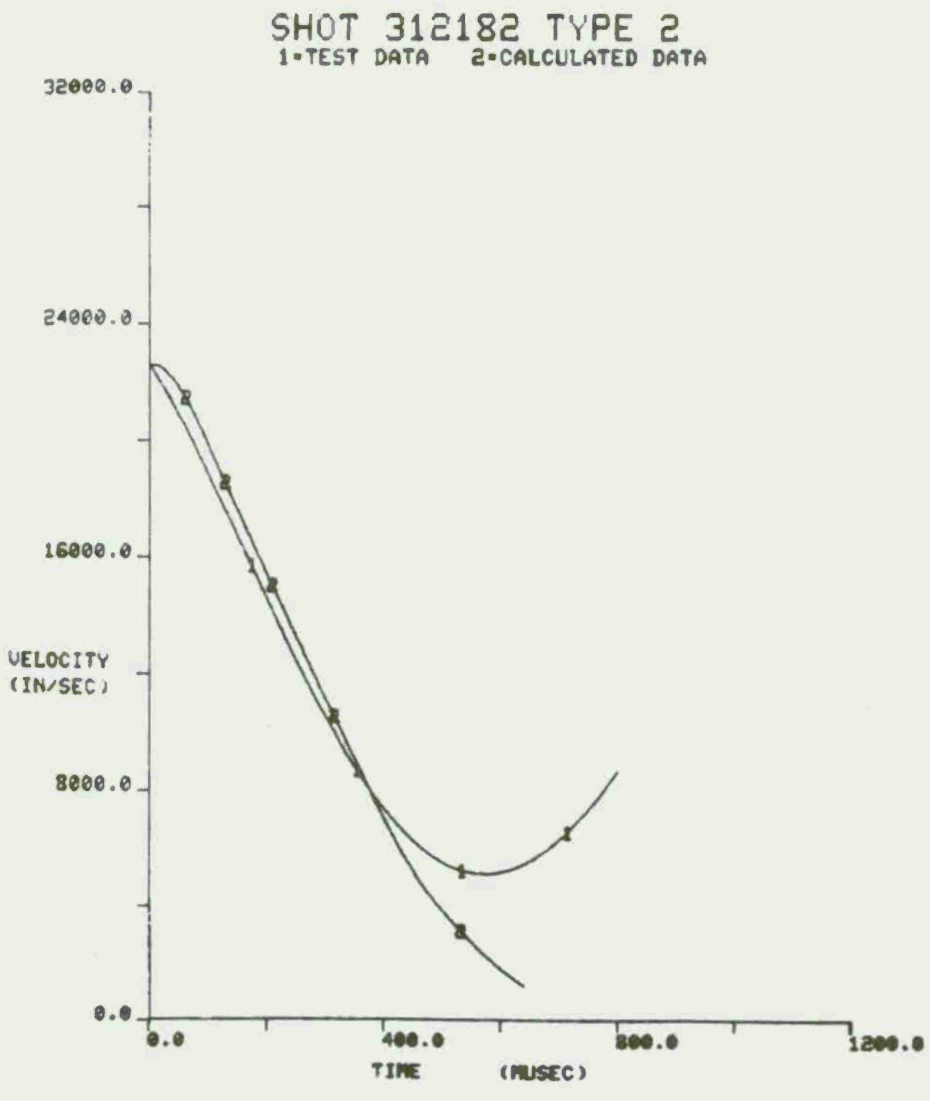

Fig 12b Velocity of Type 2, Shot 312182

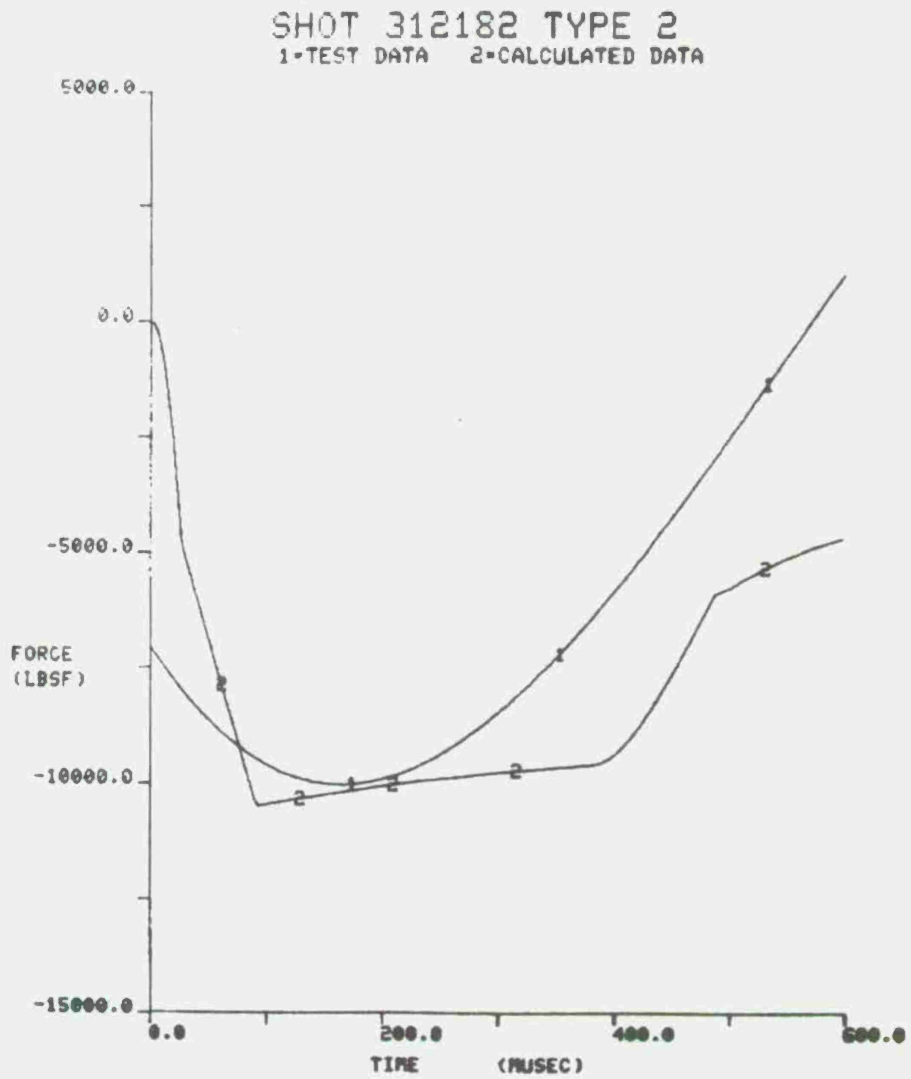

Fig 12c Force of Type 2, Shot 312182

Fig 13a Distance of Type 2, Shot 403141

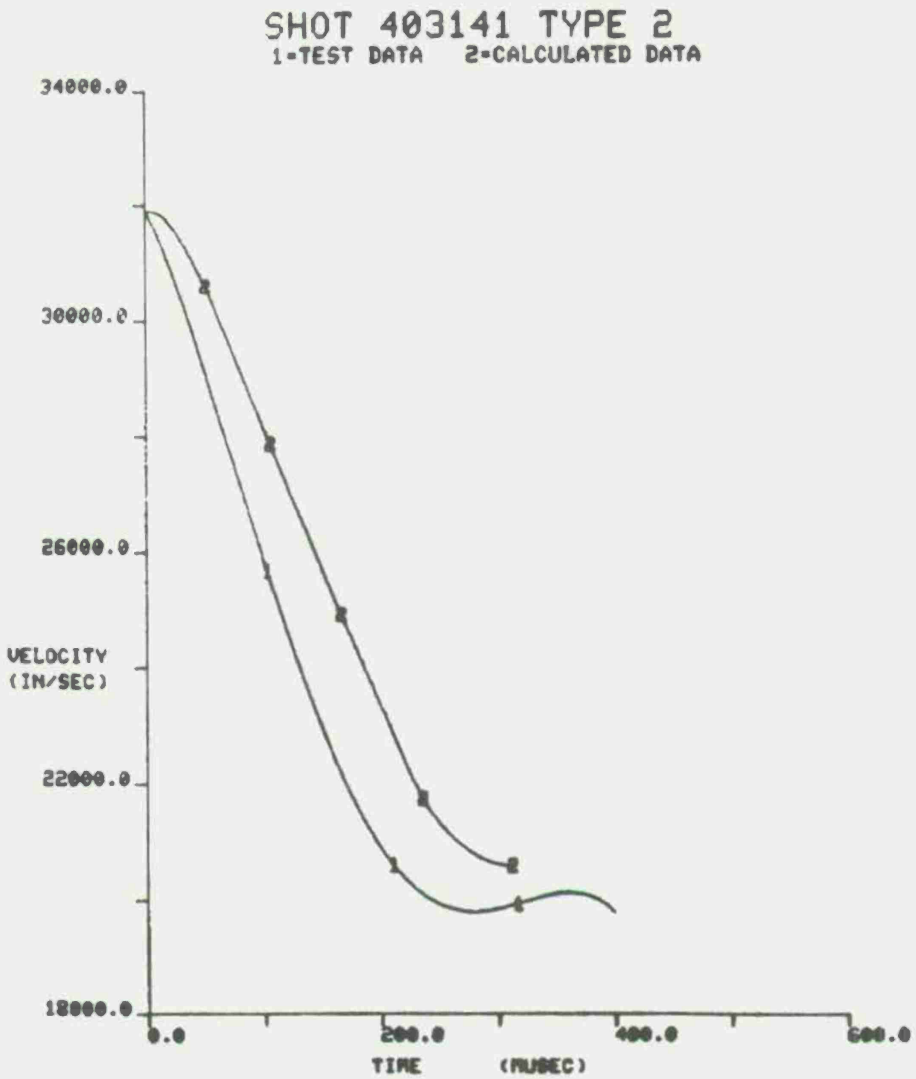

Fig 13b Velocity of Type 2, Shot 40314

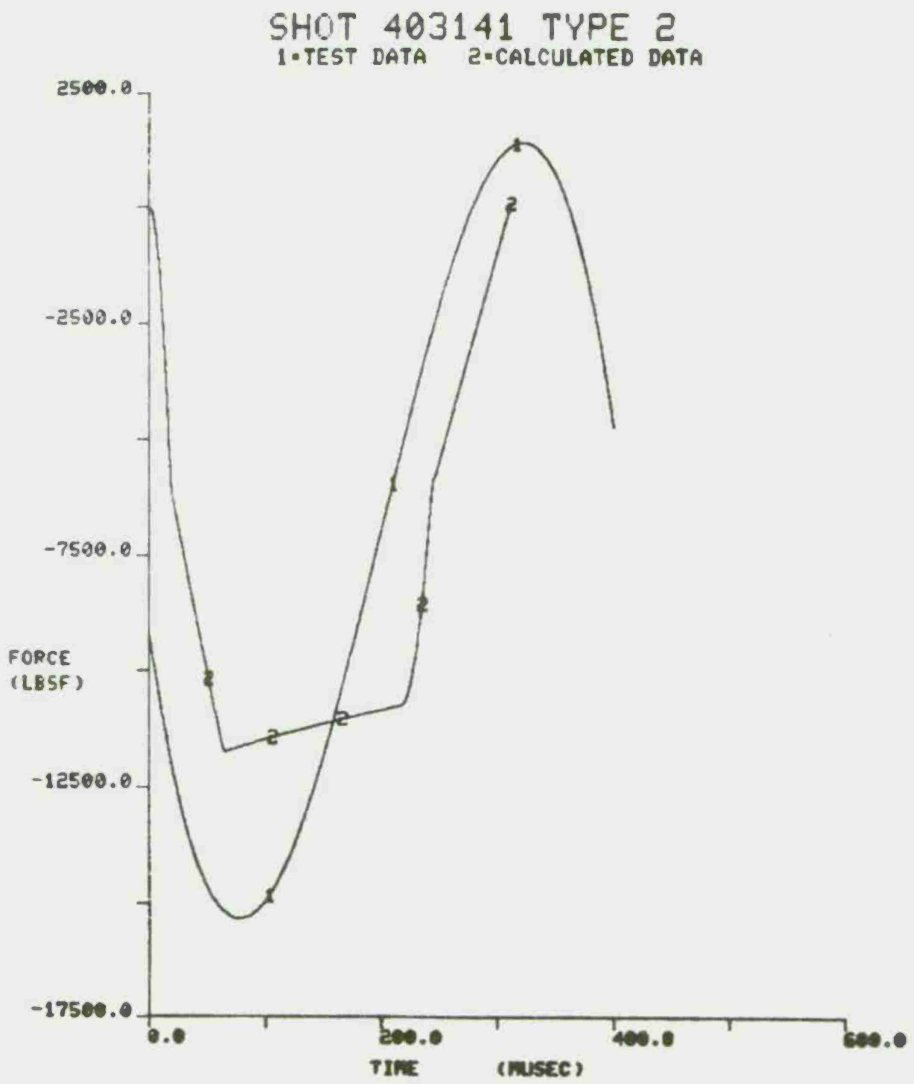

Fig 13c Force of Type 2, Shot 403141

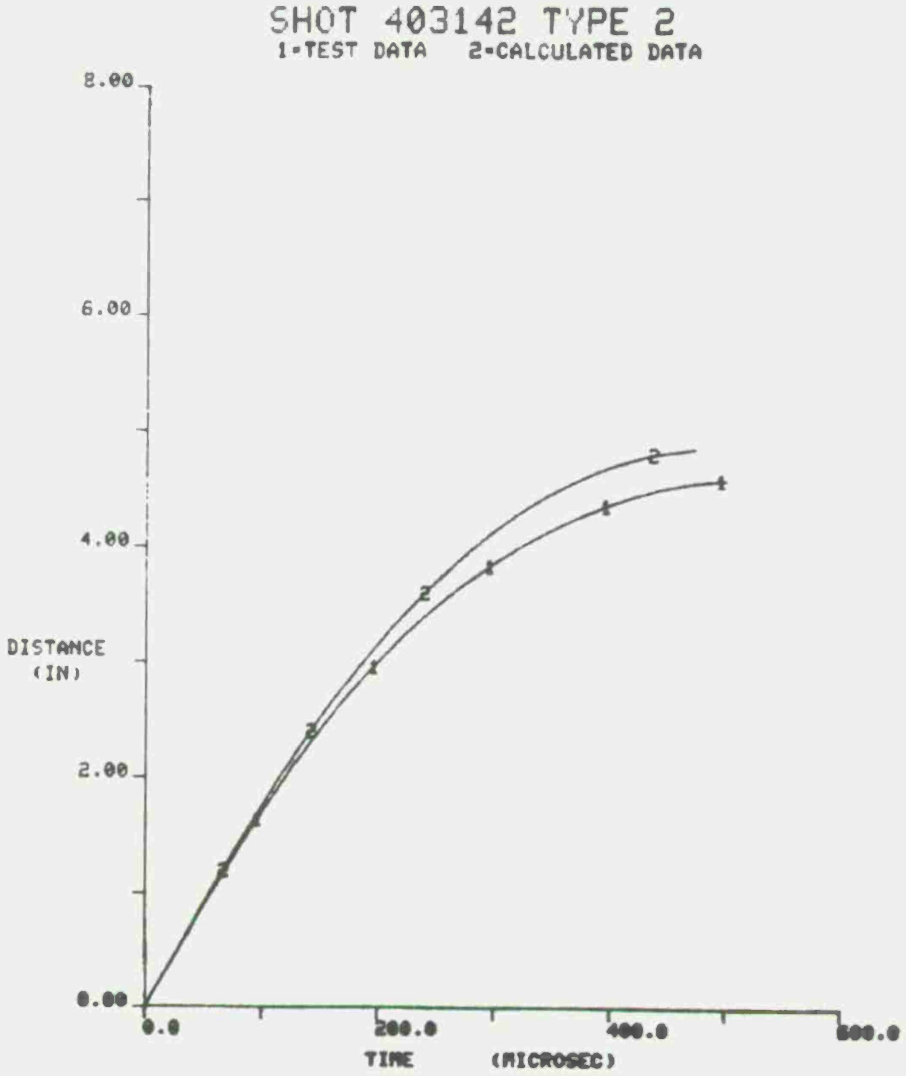

Fig 14a Distance of Type 2, Shot 403142

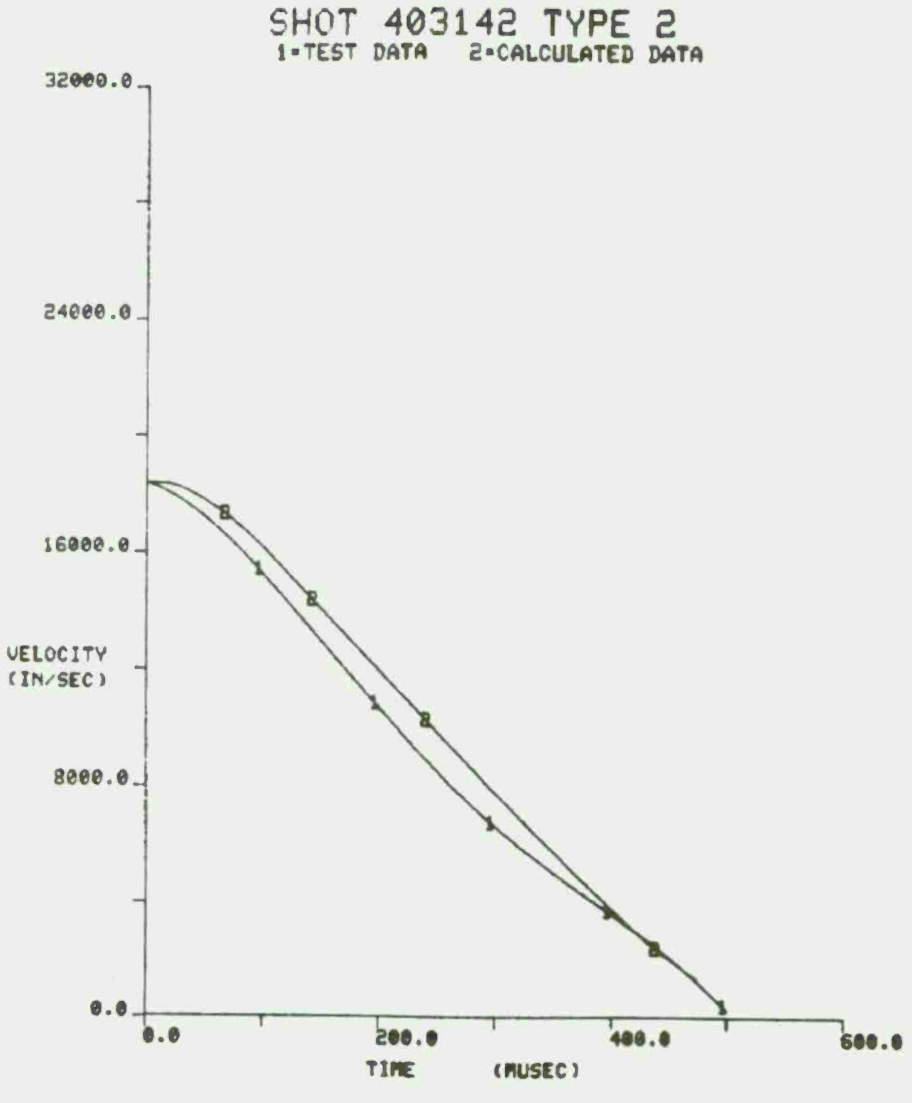

Fig 14b Velocity of Type 2, Shot 403142

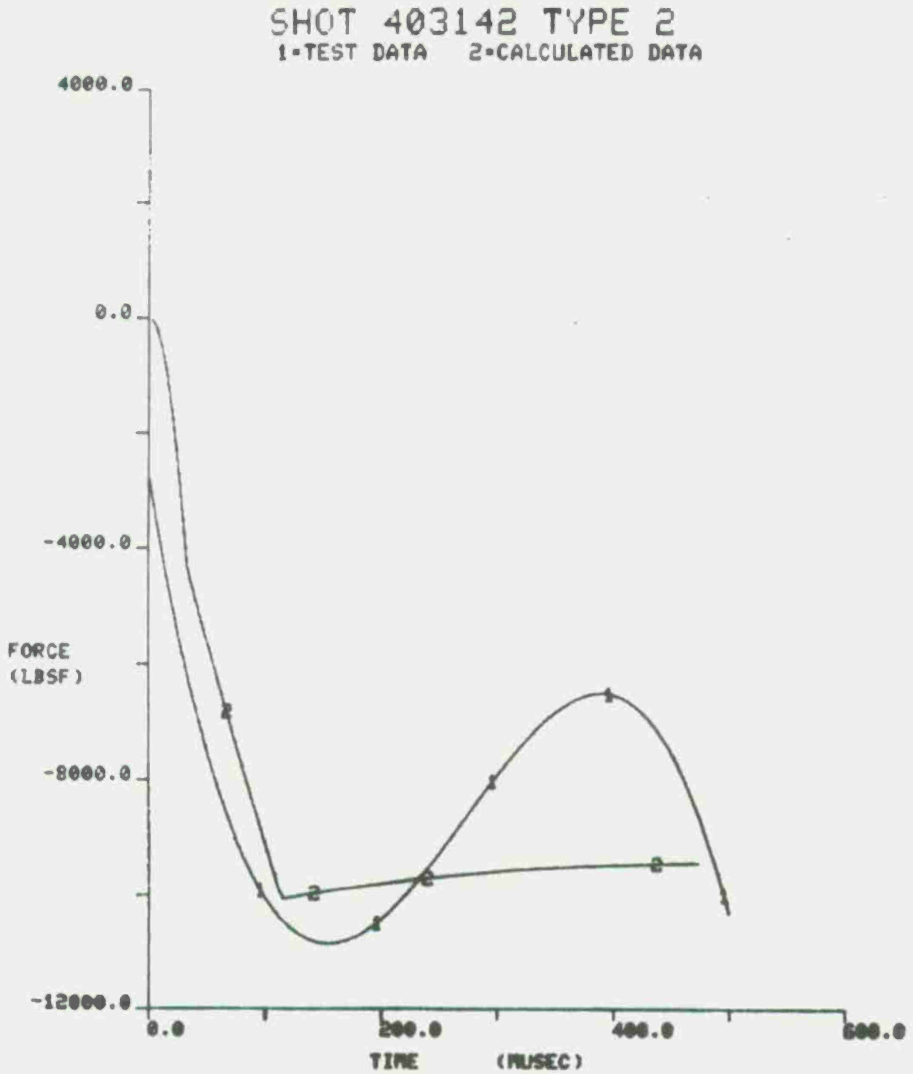

Fig 14c Force of Type 2,Shot 403142

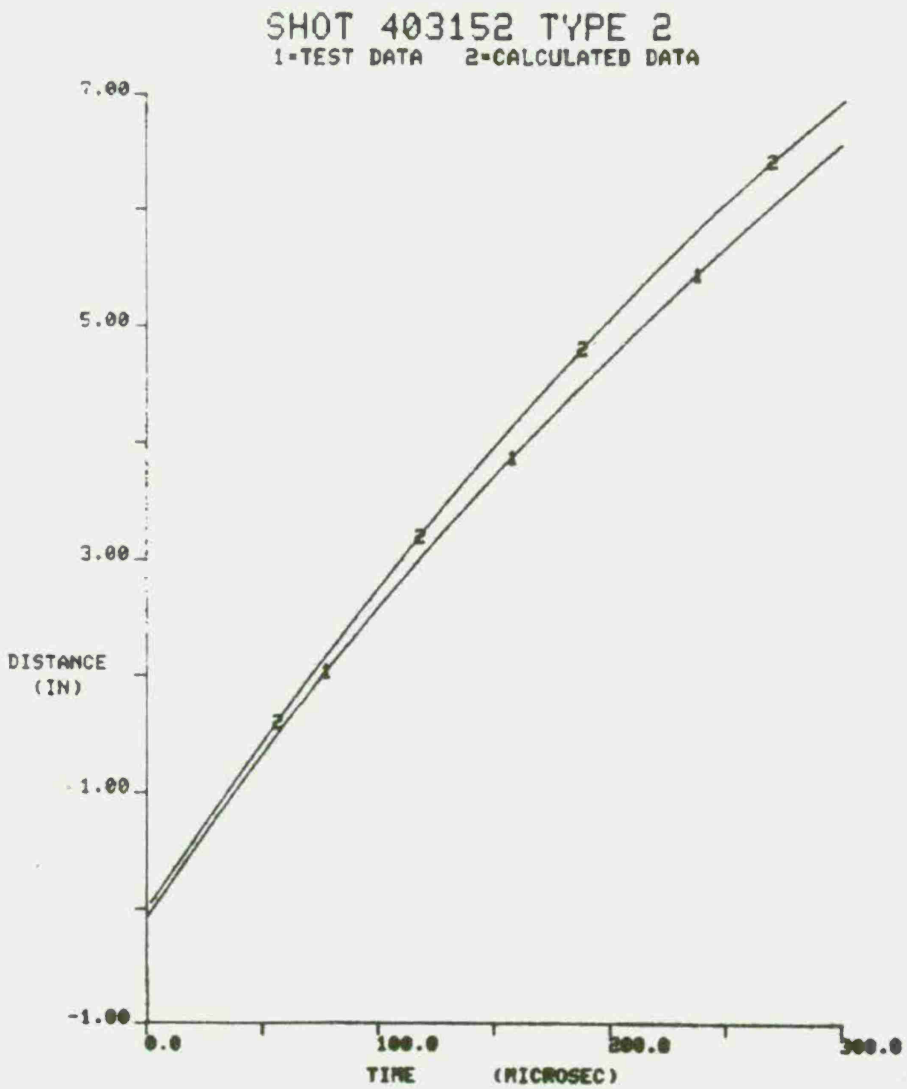

Fig 15a Distance of Type 2,Shot 403152

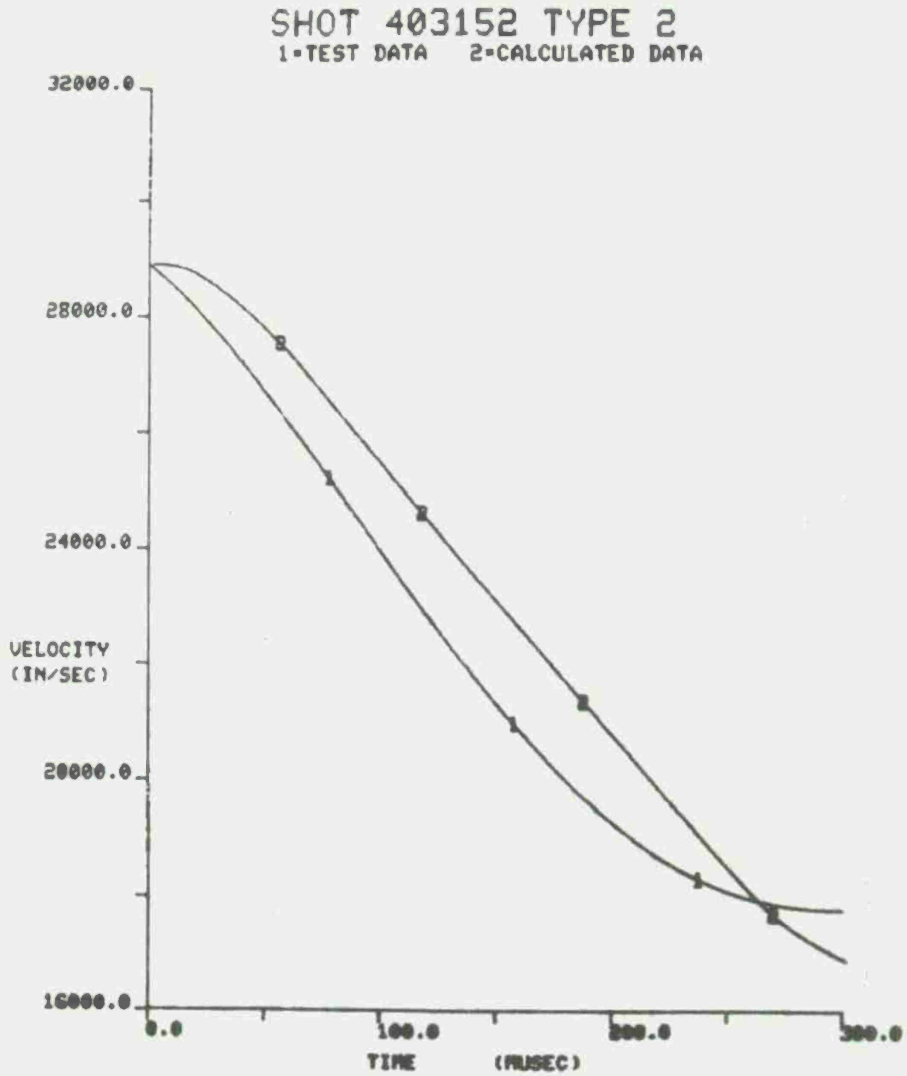

Fig 15b Velocity of Type 2, Shot 403152

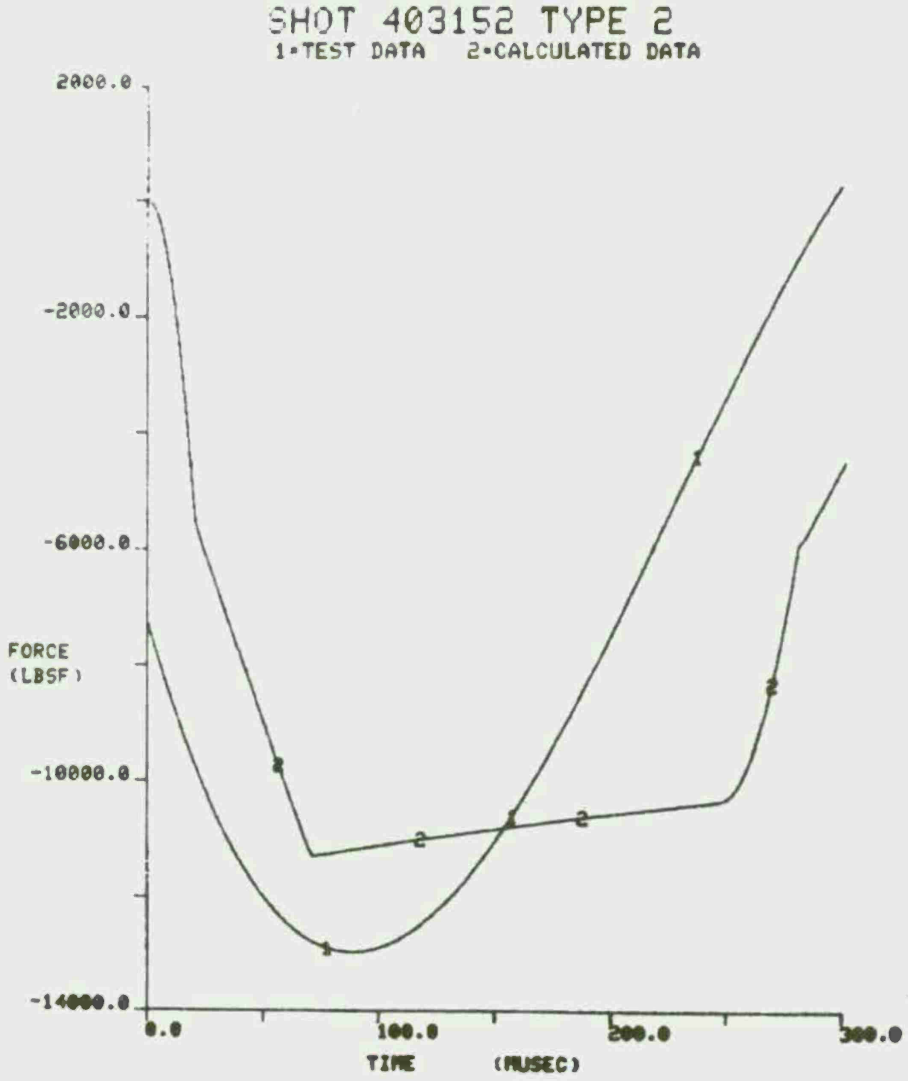

Fig 15c Force of Type 2,Shot 403152

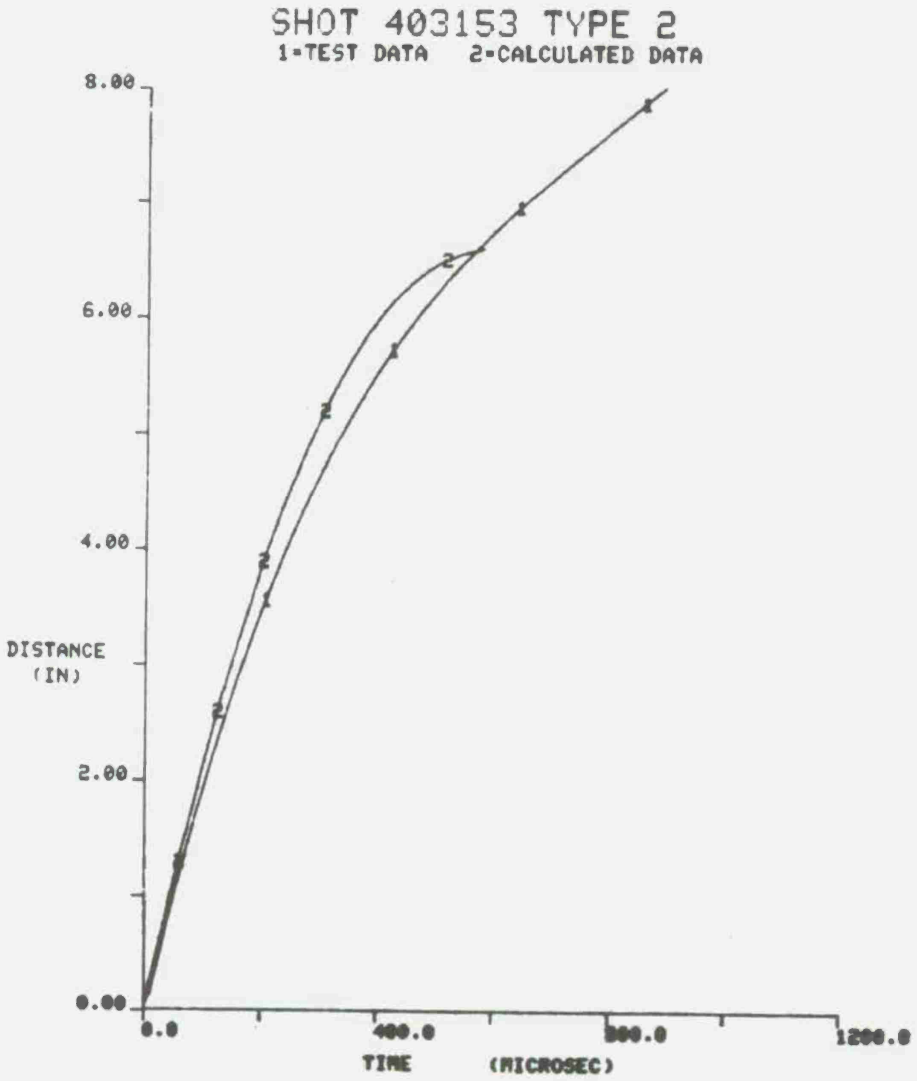

Fig 16a Distance of Type 2,Shot 403153

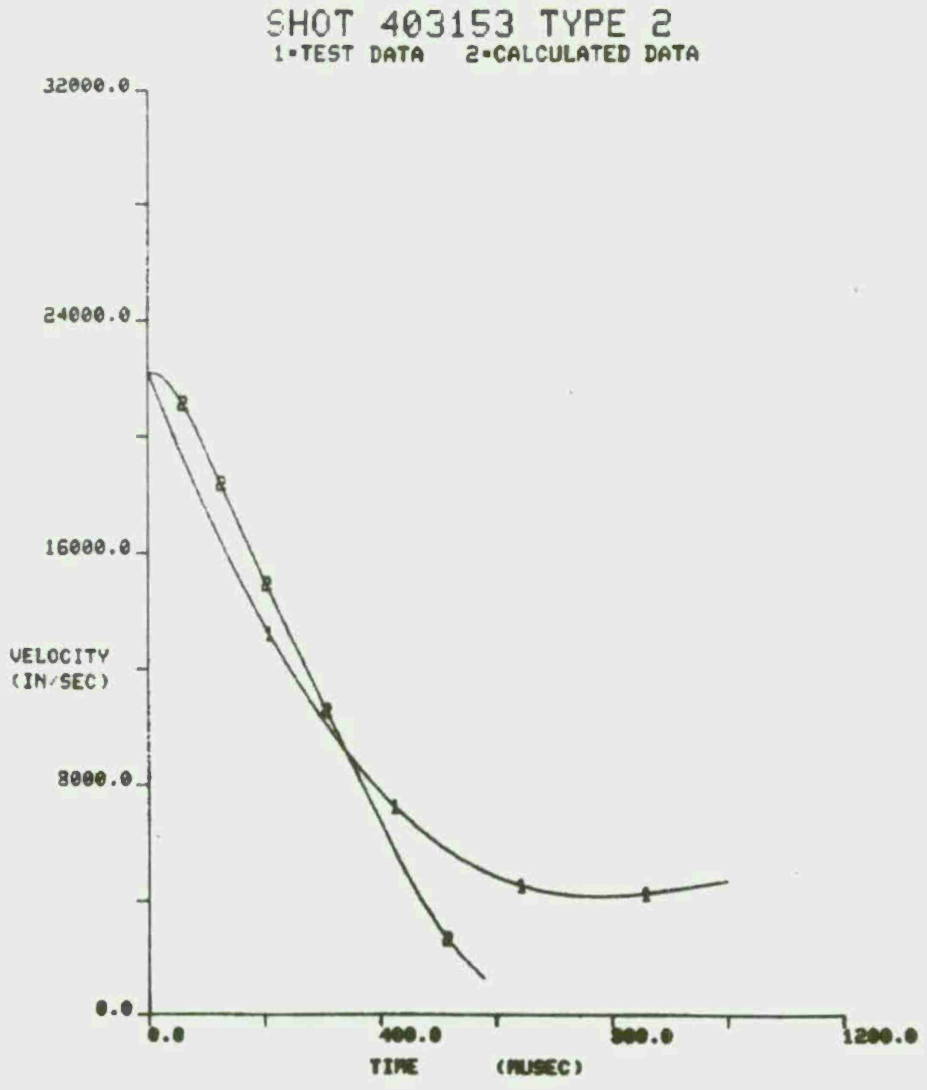

Fig 16b Velocity of Type 2,Shot 403153

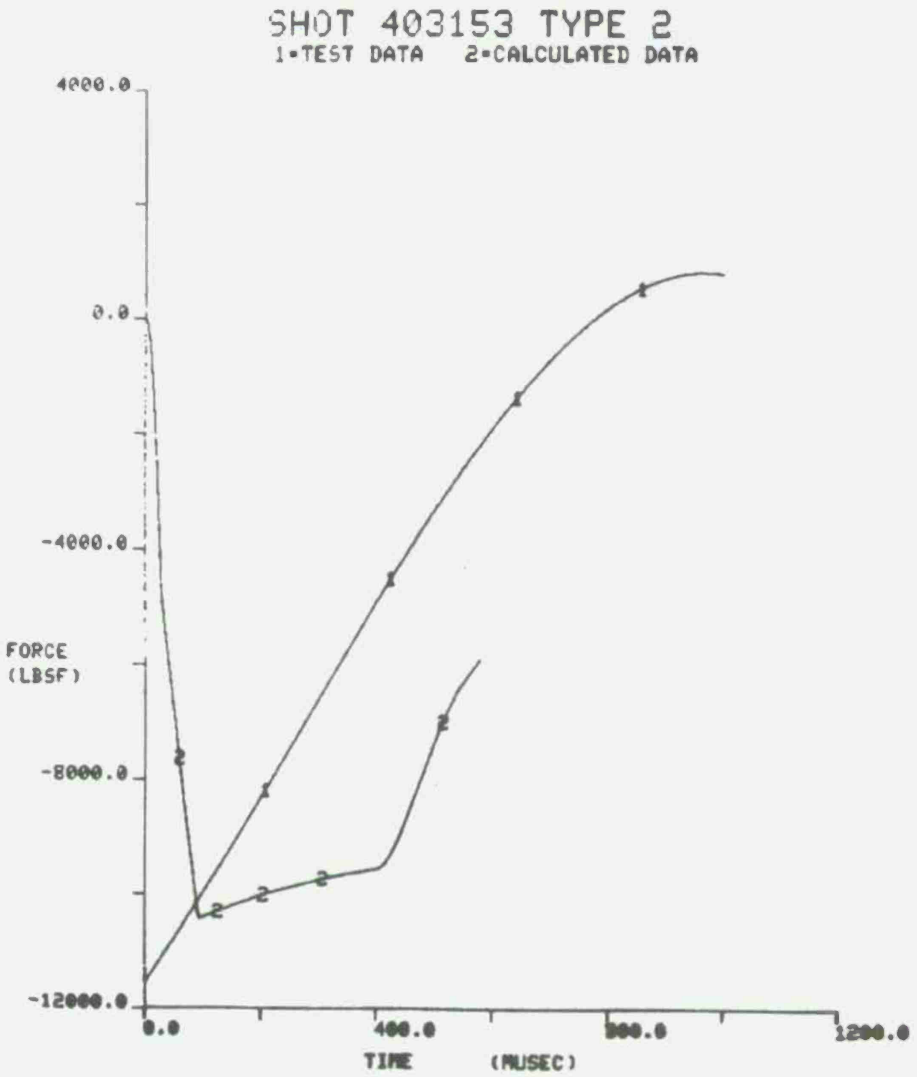

Fig 16c Force of Type 2,Shot 403153

DISTRIBUTION LIST

	Copy No.
Commander	
U.S. Army Armament Command	
ATTN: AMSAR-ASR, LTC Couniham	1
AMSAR-EN, L. Ambrosini	2
AMSAR-RD, J. Brinkman	3
AMSAR-RDT, Dr. E. Haug	4
Rock Island, IL 61201	
Commander	
U.S. Army Materiel Command	
ATTN: AMCRD-W, R. Happick	5
5001 Eisenhower Ave	
Alexandria, VA 22333	
Commander	
Picatinny Arsenal	
ATTN: SARPA-TS-S	6-10
SARPA-AD-D-A-2	11-30
SARPA-FR-S, A. Loeb	31
SARPA-FR-S-R, G. Demitrack	32
SARPA-FR, Dr. E. G. Sharkoff	33
SARPA-CO-ACP, M. Jacobson	34-48
Dover, NJ 07801	
Commander	
Watervliet Arsenal	
ATTN: SARWV-RDD, P. Rummel	49
SARWV-RT-B, Dr. Schmeideshoff	50
SARWV-RDD-SE, F. John	51
Watervliet, NY 12189	
Director	
U.S. Army Ballistic Research Laboratories	
ATTN: AMXBR-TB, Dr. J. Frasier	52
AMXBR-TB, Dr. W. Gillich	53
AMXBR-TB, Dr. E. Bloore	54
AMXBR-IB, Dr. B. Burns	55
AMXBR-LB, Bldg 305	56
Aberdeen Proving Ground, MD 21005	

Deputy Chief of Staff for Research, Development
and Acquisition
The Pentagon
ATTN: D. Hardison 57
Washington, DC 20310

President
U.S. Army Armor Engineering Board
ATTN: STEBB-TD-A 58
Fort Knox, KY 40121

Chamberlain Manufacturing Corporation
Research & Development Division
ATTN: J. Ulrich 59
East 4th & Esther Streets
Waterloo, IA 50705

Commander
Harry Diamond Laboratories
ATTN: Library 60
Washington, DC 20438

Union Carbide Corporation
Nuclear Division
Oak Ridge Y12 Plant
ATTN: T.C. Myhre, Bldg 9103 61
Oak Ridge, TN 37830

Commander
Frankford Arsenal
ATTN: SARFA-PDM, J. Katlin 62
Bridge & Tacony Streets
Philadelphia, PA 19124

Director
U.S. Army Materials & Mechanics Research Center
ATTN: AMXMR-MT, F.R. Larsen 63
Watertown, MA 02172

Redstone Scientific Information Center
U.S. Army Missile Command
ATTN: Chief, Document Section 64
Officers Training, Munitions Dept, Mr. Angeloff 65
Redstone Arsenal, AL 35809

Battelle
Pacific Northwest Laboratories
ATTN: Robert S. Kemper, Jr. 66
Battelle Boulevard
Richland, WA 99352

Kennametal, Incorporated
ATTN: O. Nichols 67
M. Simon 68
Post Office Box 231
Latrobe, PA 15650

Director
U.S. Army Materiel Systems Analysis Agency
ATTN: AMXSY-GA, G. Zeller 69
Aberdeen Proving Ground, MD 21005

U.S. Army Tank Automotive Command
ATTN: AMSTA-RHC, C. Bradley 70
Warren, Michigan 48090

Prof H. Kolsky 71
Brown University
Providence, RI 02812

Dr. I.W. Ipson 72
Dr. R.F. Recht 73
Denver Research Institute
Denver, CO 80201

Dr. S.A. Finnegan 74
Research Dept
Naval Weapons Center
China Lake, CA 93555

Prof A.C. Eringen
Continuum Mechanics Group
Princeton University
Princeton, NJ 08540 — 75

Prof W. Goldsmith
Div of Applied Mechanics
University of California
Berkeley, CA 94720 — 76

Defense Documentation Center
Cameron Station
Alexandria, VA 22314 — 77-88